JOURNAL OF GUIDANCE, CONTROL, AND DYNAMICS
Vol. 29, No. 6, November–December 2006

Sliding Mode Disturbance Observer-Based Control for a Reusable Launch Vehicle

Charles E. Hall*
NASA Marshall Space Flight Center, Huntsville, Alabama 35812
and
Yuri B. Shtessel†
University of Alabama in Huntsville, Huntsville, Alabama 35899

DOI: 10.2514/1.20151

The nation's goals to replace the aging Space Shuttle fleet and pursue exploration of our solar system and beyond will require more robust, less costly launch vehicles and spacecraft. This paper presents a novel sliding mode control approach, sliding mode control driven by sliding mode disturbance observers with gain adaptation, for a reusable launch vehicle flight control system design as a way to improve robustness to many phenomena such as modeling uncertainties and disturbances, while retaining continuity of control without using high control gains. Because of the robustness to external disturbances and modeling uncertainties, the proposed flight control system design also can reduce cost by requiring less time in design cycle and preflight analyses. This design is applied to terminal area energy management and approach/landing. The multiple-loop flight controller design features low-order disturbance observers that rely only on knowledge of the bounds of the disturbance. A gain-adaptation algorithm is included in the disturbance observer design that provides the least gain needed for existence of the sliding mode. Six degree-of-freedom computer simulations of the X-33 technology demonstration suborbital reusable launch vehicle for nominal and severe wind-gust tests demonstrate improved performance over a more conventional, classical control system design.

I. Introduction

SPACE exploration, one of NASA's primary missions, will require future launch vehicles and spacecraft to be safer, more reliable, and more affordable. To achieve these goals, NASA must continue to develop unique capabilities and facilitate the development of new technologies. This will ensure that the nation will have reliable space access for human and robotic space exploration and will enhance national security as well as commercial space activities [1].

Improvements in safety, reliability, and affordability can be attained through advanced guidance and control (AGC) technologies [2]. These new methods offer improvements in the accommodation of disturbances, uncertainties, and control system failures that would make reusable launch vehicles (RLV) much more robust and safer to fly. Many of these methods require far less time spent in design and preflight analysis, thereby reducing development and operational cost.

Many AGC methods have been investigated during the Advanced Guidance and Control Program at NASA's Marshall Space Flight Center (MSFC) [3]. Collaborating with seven universities across the country, MSFC engineers implemented advanced control system designs into the X-33 MAVERIC flight simulation for testing. MAVERIC (Marshall aerospace vehicle representation in C) [4] was developed during the X-33 program for flight dynamics analyses and contains high-fidelity models of the vehicle's aerodynamics, avionics, and flight control system actuators as well as the baseline mission manager, guidance, navigation, and control algorithms. These AGC algorithms, including the Theta-D optimal algorithm [5], adaptive control [6], trajectory linearization control [7], and continuous multiple-time-scale sliding mode control [8–12] were tested in ascent, transition, and entry regions of flight, and their performance was compared with the baseline guidance, navigation, and control algorithms [3]. Recent AGC methods for terminal area energy management and approach/land (TAL) regions of flight (Fig. 1) are available [13–15].

This work presents the first application of sliding mode disturbance observer (SMDO) driven sliding mode control (SMC) to improve RLV flight control performance in TAL.

Motivated by NASA's goals and the need to extend advanced control research in the TAL region of flight, this novel approach in sliding mode control theory, sliding mode control driven by sliding mode disturbance observers (SMC/SMDO) with gain adaptation, was developed. This is a continuous, multiple-loop design for quasi cascade systems. SMC has already been successfully applied to X-33 ascent and entry flight control [8–12], as well as in aircraft [16,17] and missile flight control [18,19]. Approximation of a sign function by a high gain-saturation function [8–12] allows a continuous quasi-SMC to be achieved, while providing convergence of the sliding variable to a zone (rather than to zero). The price for continuous control is a partial loss of robustness to disturbances and model uncertainties. Robustness may be restored by incorporating SMDO that can provide estimates of the bounded disturbances/uncertainties, which can be used in the control functions to compensate for them [20,21]. The SMDO does not rely on complete knowledge of the bounded disturbance mathematical model, just on its bounds, resulting in a simple low-order design. Remarkably, the improved robustness to external disturbances is achieved without high control gains as in [8–12]. This improves robustness of the SMC/SMDO approach to unmodeled dynamics as well. Usually, conservative estimation of these bounds yields high-amplitude switching control in the SMDO, making onboard computer implementation more difficult. Because disturbance magnitude is varying, the conservatively chosen gain used in the SMDO could also be larger than needed for estimation. This was the motivation for a gain-adaptation algorithm based on sliding modes, which provides the least gain needed for robust estimation, while making the output of the SMDO easier to filter, as an added benefit.

Presented as Paper 6145 at the Guidance, Navigation and Control Conference and Exhibit, San Fancisco, 14–18 August 2005; received 20 September 2005; revision received 5 April 2006; accepted for publication 14 April 2006.

*Aerospace Engineer, Flight Mechanics and Analysis Division; Charles.E.Hall@nasa.gov.

†Professor, Department of Electrical and Computer Engineering; shtessel@ece.uah.edu. Associate Fellow AIAA.

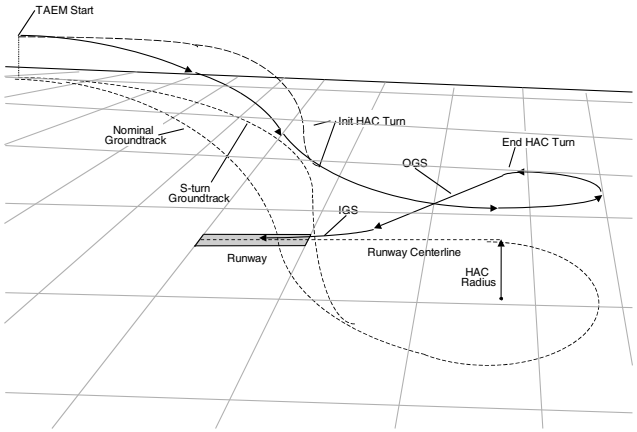

Fig. 1 Example TAEM and approach/land trajectory for an RLV.

The proposed SMC/SMDO can also offer improvements in cost-reducing the controller design cycle, because in general, only one stability analysis is needed for a particular vehicle configuration or mission design by virtue of Lyapunov stability criteria being used in the design phase of the controller. By contrast, a classical control system that relies on linear stability analysis criteria will require many stability analyses over the range of flight conditions and for each vehicle and mission design. This means far less program expense for stability analysis during the design phase and preflight for each mission when using SMC in the autopilot design. Of course, extensive high-fidelity simulations tests are required for any type of a controller in order to assess its performance characteristics.

Using the X-33 MAVERIC six-degree-of-freedom simulation with medium-fidelity vehicle subsystem models (sensors and actuators) and high-fidelity vehicle and environment models (aerodynamics and winds), it is shown that the continuous SMC/SMDO offers improved guidance command tracking in a nominal flight simulation with a realistic reference wind profile. A synthetic, severe wind-gust simulation is also presented that shows superior performance by the continuous SMC/SMDO.

This paper is structured as follows. Section II presents the continuous SMC/SMDO technique developed for robust output tracking in nonlinear MIMO systems. An application of the SMC/SMDO technique to the robust output tracking in quasicascade nonlinear systems is presented in Sec. III. Section IV presents the dynamic model of the RLV. The RLV control problem is formulated in Sec. V. Section VI presents the multiple-loop, continuous SMC/SMDO design for the RLV. The baseline X-33 flight controller design is presented in Sec. VII. The results of the X-33 flight simulations in TAL flight are discussed and analyzed in Sec. VIII. Finally, Sec. IX presents the conclusions.

II. Continuous Sliding Mode Control Driven by a Sliding Mode Disturbance Observer

This section presents a continuous SMC technique based on an SMDO that is applied to robust output tracking in linearizable MIMO systems with nonlinear feedback.

Consider a nonlinear MIMO system [22]

$$\dot{\boldsymbol{x}} = \boldsymbol{f}(\boldsymbol{x}, t) + \boldsymbol{G}(\boldsymbol{x}, t)\boldsymbol{u}, \qquad \boldsymbol{y} = \boldsymbol{h}(\boldsymbol{x}, t) \tag{1}$$

where

$$\boldsymbol{f}(\boldsymbol{x}, t) \in \Re^n, \qquad \boldsymbol{h}(\boldsymbol{x}, t) = [h_1, h_2, \ldots, h_m]^T \in \Re^m,$$
$$\boldsymbol{G}(\boldsymbol{x}, t) = [\boldsymbol{g}_1, \boldsymbol{g}_2, \ldots \boldsymbol{g}_m] \in \Re^{n\times m}, \qquad \boldsymbol{x} \in \Re^n, \qquad \boldsymbol{y} \in \Re^m,$$
$$\boldsymbol{u} \in \Re^m, \qquad \boldsymbol{g}_i \in \Re^n \forall\ i = 1, \ldots, m$$

are analytic vector and matrix functions. Assuming the system (1) is completely feedback linearizable [22] in a reasonable compact domain $\boldsymbol{x} \in \Gamma(\boldsymbol{x})$, the system can be transformed to a regular format:

$$\begin{bmatrix} \boldsymbol{y}_1^{(r_1)} \\ \boldsymbol{y}_2^{(r_2)} \\ \ldots \\ \boldsymbol{y}_m^{(r_m)} \end{bmatrix} = \begin{bmatrix} L_f^{r_1} h_1(\boldsymbol{x}, t) \\ L_f^{r_2} h_2(\boldsymbol{x}, t) \\ \ldots \\ L_f^{r_m} h_m(\boldsymbol{x}, t) \end{bmatrix} + \boldsymbol{E}(\boldsymbol{x}, t)\boldsymbol{u},$$

$$\boldsymbol{E}(\boldsymbol{x}, t) = \begin{bmatrix} L_{g_1}(L_f^{r_1-1}h_1) & L_{g_2}(L_f^{r_1-1}h_1) & \ldots & L_{g_m}(L_f^{r_1-1}h_1) \\ L_{g_1}(L_f^{r_2-1}h_2) & L_{g_2}(L_f^{r_2-1}h_2) & \ldots & L_{g_m}(L_f^{r_2-1}h_2) \\ \ldots & \ldots & \ldots & \ldots \\ L_{g_1}(L_f^{r_m-1}h_m) & L_{g_2}(L_f^{r_m-1}h_m) & \ldots & L_{g_m}(L_f^{r_m-1}h_m) \end{bmatrix} \tag{2}$$

where $|\boldsymbol{E}(\boldsymbol{x}, t)| \neq 0 \quad \forall\ \boldsymbol{x} \in \Gamma$, $L_f^{r_i} h_i$, and $L_{g_i}(L_f^{r-1}h_i) \quad \forall\ i = 1, \ldots, m$ are corresponding Lie derivatives [22], and $\bar{\boldsymbol{r}} = [r_{1,}, r_2, \ldots, r_m]^T$ is a vector relative degree.

To achieve decoupled asymptotic output tracking in systems (1) and (2) by means of control $\boldsymbol{u}$, the desired decoupled output tracking and compensated dynamics are introduced:

$$\sigma_i = e_i^{(r_i-1)} + c_{i,r_i-2}e_i^{(r_i-2)} + \ldots + c_{i,1}e_i^{(1)} + c_{i,0}e_i + c_{i,-1}e_{i,-1} = 0$$
$$\forall\ i = 1, \ldots, m \tag{3}$$

where

$$e_i = y_{i,c}(t) - y_i(t)$$

$y_{i,c}(t)$ is the ith output command profile:

$$e_i^{(j)} = \mathrm{d}^j e_i / \mathrm{d}t^j, \qquad e_{i,-1} = \int e_i \,\mathrm{d}t$$

and the coefficients

$$c_{i,j} \quad \forall\ i = \mathbf{1}, \ldots, m \quad \forall\ j = -\mathbf{1}, \ldots, r_i - \mathbf{2}$$

are chosen to achieve the desired eigenvalue placement in the decoupled differential–integral equations (3). In terms of sliding mode control [20],

$$\boldsymbol{\sigma} = [\sigma_1, \sigma_2, \ldots, \sigma_m]^T \in \Re^m$$

is called a vector *sliding variable*, and Eq. (3), $\boldsymbol{\sigma} = \mathbf{0}$, is called a *sliding surface*.

The sliding variable dynamics are derived

$$\dot{\boldsymbol{\sigma}} = \boldsymbol{\Psi}(.) - \boldsymbol{E}(\boldsymbol{x}, t)\boldsymbol{u} \tag{4}$$

where

$$\boldsymbol{\Psi}(.) = [\psi_1(.), \ldots, \psi_m(.)]^T \Re^m,$$
$$\psi_i(.) = y_{i,c}^{(r_i)} + c_{i,r_i-2}e_i^{(r_i-1)} + \cdots + c_{i,1}e_i^{(2)} + c_{i,0}e_i^{(1)}$$
$$+ c_{i,-1}e_i - L_f^{r_i} h_i(x, t) \quad \forall\ i = 1, \ldots, m$$

To separate the control design into m SISO control designs, a new control variable is introduced:

$$\tilde{\boldsymbol{u}} = \boldsymbol{E}(\boldsymbol{x})\boldsymbol{u} \tag{5}$$

This allows Eq. (4) to be rewritten in a scalar format:

$$\dot{\sigma}_i = \psi_i^0(.) + \Delta\psi_i(.) - \tilde{u}_i \tag{6}$$

where

$$\tilde{\boldsymbol{u}} = [\tilde{u}_1, \ldots, \tilde{u}_m]^T, \qquad \boldsymbol{\Psi}(.) = \boldsymbol{\Psi}^0(.) + \Delta\boldsymbol{\Psi}(.)$$

with

$$\boldsymbol{\Psi}^0(.) = [\psi_1^0(.), \ldots, \psi_m^0(.)]^T \in \Re^m$$

and

$$\Delta\mathbf{\Psi}(.) = [\Delta\psi_1(.), \ldots, \Delta\psi_m(.)]^T \in \Re^m$$

are known and unknown (due to external disturbances and model uncertainties) vectors, respectively. The unknown vector is assumed bounded, that is,

$$\|\Delta\psi_i(.)\| \le L_i \quad \forall\ i = 1, \ldots, m \quad \forall\ \boldsymbol{x} \in \Gamma$$

The problem is to design a *continuous* SMC u that provides decoupled asymptotic output tracking: $e_i(t) \to 0$ as time increases, by guaranteeing stability to the sliding variable dynamics [Eqs. (4) or (6)] in the presence of unknown bounded disturbances and uncertainties.

Once the control $\tilde{\boldsymbol{u}}$ is identified in Eq. (6), the original control law $\boldsymbol{u}$ can be easily computed based on Eq. (5) as

$$\boldsymbol{u} = \boldsymbol{E}^{-1}(\boldsymbol{x})\tilde{\boldsymbol{u}} \tag{7}$$

To design an SMDO for estimating the bounded disturbance $\Delta\psi_i(.)$, auxiliary sliding variables are introduced:

$$s_i = \sigma_i + z_i, \qquad \dot{z}_i = -\psi_i^0 + \tilde{u}_i - v_i \tag{8}$$

The s_i dynamics are derived, taking into account Eqs. (6) and (8):

$$\dot{s}_i = \Delta\psi_i - v_i \tag{9}$$

A. SMDO Based on Traditional SMC

A simple Lyapunov-based analysis [20] shows that the auxiliary sliding variables s_i are stabilized at zero by means of auxiliary traditional SMC, v_i, in finite time:

$$v_i = (L_i + \rho_i)\text{sign}(s_i), \qquad \rho_i > 0 \tag{10}$$

Indeed, by introducing a Lyapunov-candidate function

$$V_i = \tfrac{1}{2}s_i^2 \tag{11}$$

and computing its derivative using Eqs. (9) and (10)

$$\dot{V}_i = s_i\dot{s}_i = s_i(\Delta\psi_i - v_i) \le |s_i|L_i - |s_i|(L_i + \rho_i) = -\rho_i|s_i| \tag{12}$$

one can conclude that $s_i \to 0$ in finite time, that is,

$$t_{ri} \le |s_i(0)|/\rho_i$$

via SMC of Eq. (10).

Therefore, equivalent control v_{ieq} estimates exactly the disturbance

$$\Delta\psi_i(.) \quad \forall\ t \ge t_{ri}$$

that is, $v_{ieq} = \Delta\psi_i(.)$ [see SMDO in Eqs. (8–10)]. To compute v_{ieq}, high-frequency switching control [Eq. (10)] can be processed by a low-pass filter (LPF) [23,24] with the transfer function given by $G_{\text{LPF}}(s)$:

$$\hat{v}_{ieq}(s) = G_{\text{LPF}}(s)v_i(s) \tag{13}$$

where s is a Laplace variable.

The signal $\hat{v}_{ieq}$ can estimate v_{ieq} and, consequently, the disturbance $\Delta\psi_i(.)$ asymptotically, in a case of nonpiecewise constant disturbances, or with a small error that is proportional to the time constant of $G_{\text{LPF}}(s)$. For instance, if $G_{\text{LPF}}(s)$ is implemented as a simple first-order lag block [24]

$$\hat{v}_{ieq}(s) = \frac{1}{\tau_i s + 1}v_i(s) \tag{14}$$

then

$$\|v_{ieq} - \hat{v}_{ieq}\| < \mathcal{O}(\tau_i)$$

and, consequently,

$$\|\Delta\psi_i - \hat{v}_{ieq}\| < \mathcal{O}(\tau_i)$$

as time increases. It is worth noting that the time constant of the filter can be taken very small, having a duty cycle of control [Eq. (10)]. This is dictated mostly by the time increment of an onboard computer, as a lower boundary [20,24].

Therefore, the disturbance $\Delta\psi_i$ is estimated by the SMDO [Eqs. (8–12)] as $\Delta\hat{\psi}_i = \hat{v}_{ieq}$. Because the SMDO based on traditional SMC [Eqs. (8–10), (13), and (14)] is a computational algorithm and does not spend any real control resources, high-frequency switching feedback v_i in Eq. (10) could be implemented with any required amplitude $L_i + \rho_i$ to preserve existence of the sliding mode in the SMDO [Eqs. (8–10), (13), and (14)].

The gain, $L_i + \rho_i$, used in the SMDO feedback SMC [Eq. (10)] is too conservative because it is meant to dominate over the disturbance $\Delta\psi_i$, which is not known but bounded:

$$|\Delta\psi_i| \le L_i$$

Because a real $G_{\text{LPF}}(s)$, for instance, given by Eq. (14), does not reject high-frequency switching components of the signal v_i in Eq. (10), but only attenuates it, it makes sense for the amplitude of v_i to be as small as possible. An adaptation algorithm would allow the gain $(L_i + \rho_i)$ to decrease in accordance with the varying disturbance, making the control easier to filter, as an added benefit.

The *gain-adaptation algorithm* proceeds as follows. Consider an SMDO with a "relaxed" feedback SMC control law [Eq. (10)] given by

$$v_i = (|\Delta\psi_i| + \rho_i)\text{sign}(s_i), \qquad \rho_i > 0 \tag{15}$$

The Lyapunov function derivative estimate in Eq. (12) is revised after substituting Eq. (15) into Eq. (12):

$$\begin{aligned}\dot{V}_i &= s_i\dot{s}_i \\ &= s_i(\Delta\psi_i - v_i) \le |s_i||\Delta\psi_i| - |s_i|(|\Delta\psi_i| + \rho_i) \\ &= -\rho_i|s_i|\end{aligned} \tag{16}$$

So, one can conclude that $s_i \to 0$ in a finite time,

$$t_{ri} \le |s_i(0)|/\rho_i$$

via the relaxed SMC [Eq. (15)]. Although outside the auxiliary sliding surface $s_i = 0$ (i.e., in a reaching phase), the more "aggressive" control law [Eq. (10)] must be used to drive the auxiliary sliding variable s_i to zero. On the other hand, $\Delta\psi_i(.) = v_{ieq}$, while in the sliding mode $s_i = 0$, and equivalent control v_{ieq} is easily estimated by means of low-pass filtering [Eq. (13) and (14)]. Therefore, in the sliding mode, $s_i = 0$, the SMDO feedback control [Eq. (15)] can be implemented as

$$v_i = (|\hat{v}_{ieq}| + \rho_i)\text{sign}(s_i), \qquad \rho_i > 0 \tag{17}$$

Filtering the high-frequency switching control [Eq. (17)] with amplitude less than the one in Eq. (10) yields better high-frequency switching amplitude attenuation for the same $G_{\text{LPF}}(s)$ in Eqs. (13) and (14). Finally, the revised SMDO with gain adaptation is implemented as

$$v_i = \begin{cases} (L_i + \rho_i)\text{sign}(s_i), & \text{if } |s_i| > \mu_i \\ (|\hat{v}_{ieq}| + \rho_i & \text{if } |s_i| \le \mu_i \end{cases} \tag{18}$$

where $\mu_i \sim \Delta T$ (ΔT is an onboard computer time increment). The SMDO in Eqs. (8), (9), (13), (14), and (18) is called an adaptive-gain SMDO.

The continuous SMC/SMDO $\tilde{u}_i$ given by Eqs. (8–10), (13), and (14) that asymptotically stabilizes the sliding variable σ_i in the presence of an unknown bounded disturbance $\Delta\psi_i(.)$ is designed as follows:

$$\tilde{u}_i = \psi_i^0(.) + K_{0i}\sigma_i + \hat{v}_{ieq} \tag{19}$$

Substituting Eq. (19) into Eq. (6) we obtain

$$\dot{\sigma}_i = -K_{0i}\sigma_i + \vartheta_i(.), \qquad \vartheta_i(.) = -\hat{v}_{ieq} + \Delta\psi_i(.) \tag{20}$$

As time increases, Eq. (20) tends to

$$\dot{\sigma}_i = -K_{0i}\sigma_i + \mathcal{O}(\tau_i), \qquad K_{0i} > 0 \tag{21}$$

because

$$\|\vartheta_i(.)\| = \|\Delta\psi_i - \hat{v}_{ieq}\| < \mathcal{O}(\tau_i) \ll L_i$$

Next, we consider stabilization of the original sliding variable σ_i in Eq. (6). This is done by means of a continuous high gain control

$$\tilde{u}_i = \psi_i^0(.) + \tilde{K}_{0i}\sigma_i$$

to a given domain, $|\sigma_i| < \varepsilon_i$. Introducing a Lyapunov function candidate

$$V_i = \tfrac{1}{2}\sigma_i^2$$

and computing its derivative, the σ_i dynamics are derived in the form

$$\dot{\sigma}_i = -\tilde{K}_{0i}\sigma_i + \Delta\psi_i(.) \tag{22}$$

We obtain the inequality

$$\tilde{K}_{0i} > \frac{L_i}{\varepsilon_i} \tag{23}$$

which gives a condition for σ_i convergence to a given domain $|\sigma_i| < \varepsilon_i$. Similar conditions for the continuous SMC/SMDO given by Eq. (19) may be derived. The same Lyapunov-based analysis yields the following lower border for the gain $\tilde{K}_{0i}$:

$$\tilde{K}_{0i} > \frac{\mathcal{O}(\tau_i)}{\varepsilon_i} \tag{24}$$

Remark 1: Inequality (24) gives a condition for σ_i convergence to a domain $|\sigma_i| < \varepsilon_i$ for the continuous SMC/SMDO. Because $\mathcal{O}(\tau_i) \ll L_i$, use of continuous SMC/SMDO is preferable because the same stabilization accuracy may be achieved via continuous control but with much lower control gain.

This property of continuous SMC/SMDO is very important in practical implementations. For instance, assume that the control $\tilde{u}_i$ provides the unmodeled, stable (actuator) second-order linear dynamics as input. This is given by

$$\tilde{u}_{iout}^{(2)} + a_i\tilde{u}_{iout}^{(1)} + b_i\tilde{u}_{iout} = b_i\tilde{u}_i, \qquad a_i > 0, \qquad b_i > 0 \tag{25}$$

where $\tilde{u}_{iout}$ is an output of the ith unmodeled dynamics. Then the unperturbed σ_i dynamics [Eq. (6)], with $\Delta\psi_i(.) = 0$ and control

$$\tilde{u}_i = \psi_i^0(.) + K_{0i}\sigma_i$$

becomes

$$\sigma_i^{(3)} + a_i\sigma_i^{(2)} + b_i\sigma_i^{(1)} + b_i\tilde{K}_{0i}\sigma_i = 0, \qquad a_i > 0, \qquad b_i > 0 \tag{26}$$

The well-known stability condition for system (26) being combined with inequalities (23) and (24) yields

$$\frac{L_i}{\varepsilon_i} < \tilde{K}_{0i} < a_i \tag{27}$$

for continuous high gain control and

$$\frac{\mathcal{O}(\tau_i)}{\varepsilon_i} < \tilde{K}_{0i} < a_i \tag{28}$$

for the continuous SMC/SMDO. Because $\mathcal{O}(\tau_i) \ll L_i$, the interval (27) is much more narrow than in Eq. (28). Furthermore, for some given a_i (unmodeled actuator dynamics) and ε_i, the interval (27) can be empty while the interval (22) is not. In this case, the continuous high gain controller makes the system (26) unstable, while the continuous SMC/SMDO retains stability.

B. SMDO Based on Super-Twisting High (Second) Order SMC

The auxiliary sliding surface dynamics [Eq. (9)] can also be stabilized by so-called supertwisting control [22]. This control belongs to a class of higher-order sliding mode control (HOSM) algorithms, which are applicable to systems with arbitrary relative degree (with respect to a sliding variable). HOSM techniques are able to stabilize not only the sliding variable to zero, but also its $k-1$ successive derivatives (i.e., kth-order HOSM). The well-known chattering effect is significantly reduced, because high-frequency switching is hidden in the higher derivative of the sliding variable. Being implemented in discrete time, HOSM provides for sliding accuracy proportional to the kth power of time increment ΔT, which makes HOSM an enhanced-accuracy robust control technique applicable to controllers and to observer design. To estimate $\Delta\psi_i(.)$, the continuous second-order sliding mode control (SOSM) [25], in particular, a supertwisting algorithm, may be used to stabilize the auxiliary sliding variable s_i in Eq. (9) to zero with robustness and in a finite time. This is done, of course, in the presence of the bounded disturbance $\Delta\psi_i(.)$.

Supertwisting SOSM control [25] is based on the analysis of the perturbed nonlinear differential equation

$$\dot{\chi} + \varpi_1|\chi|^{1/2}\mathrm{sign}(\chi) + \varpi_2\int \mathrm{sign}(\chi)\,\mathrm{d}\tau = \xi(t), \qquad |\dot{\xi}(t)| \le C \tag{29}$$

It is well known [25] that a solution $\chi(t)$ of Eq. (29) and its derivative $\dot{\chi}(t)$ converge to zero in finite time

$$\tilde{t}_r \le \frac{7.6\chi(0)}{\varpi_2 - C}$$

if $\varpi_1 = 1.5\sqrt{C}$ and $\varpi_2 = 1.1C$, then

$$T \le \frac{7.6z_0'}{\alpha_1 - C}$$

Substituting the following supertwist control

$$v_i = \varpi_{1i}|s_i|^{1/2}\mathrm{sign}(s_i) + \varpi_{2i}\int \mathrm{sign}(s_i)\,\mathrm{d}\tau \tag{30}$$

into Eq. (9), the s_i−compensated dynamics are achieved

$$\dot{s}_i + \varpi_{1i}|s_i|^{1/2}\mathrm{sign}(s_i) + \varpi_{2i}\int \mathrm{sign}(s_i)\,\mathrm{d}\tau = \Delta\psi_i(.) \tag{31}$$

Assuming

$$|\Delta\dot{\psi}_i(.)| \le \bar{L}_i$$

and comparing Eqs. (29) and (31), one can conclude that selecting parameters of the supertwist controller [Eq. (30)] that satisfy $\varpi_{1i} = 1.5\sqrt{\bar{L}_i}$ and $\varpi_{2i} = 1.1\bar{L}_i$ will imply that the auxiliary sliding variable and its derivative will converge to zero, that is, $s_i, \dot{s}_i \to 0$, in finite time,

$$\tilde{t}_r \le \frac{7.6s_i(0)}{\varpi_{2i} - \bar{L}_i}$$

using the control [Eq. (30)]. Note that the control function v_i in Eq. (30) is continuous because the discontinuous terms $\mathrm{sign}(s_i)$ are integrated. Finally, $v_i(t) = \Delta\psi_i(.)$ in the second-order sliding mode ($s_i = \dot{s}_i = 0$), and the continuous supertwist control $v_i(t)$ will

estimate exactly the disturbance $\Delta\psi_i(.)$. Next, the original continuous SMC driven by supertwist SMDO yields

$$\tilde{u}_i = \psi_i^0(.) + K_{0i}\sigma_i + v_i \tag{32}$$

and the original sliding variable σ_i compensated dynamics become

$$\dot{\sigma}_i = -K_{0i}\sigma_i, \quad \forall\ t > \tilde{t}_r \tag{33}$$

It is obvious that $\sigma_i \to 0$ asymptotically in the presence of bounded disturbance $\Delta\psi_i(.)$ by means of the continuous SMC driven by supertwist SMDO. The rate of convergence is controlled by the value $K_{0i} > 0$.

Finally, we can conclude that the proposed SMDO algorithms based on traditional SMC [Eqs. (8–10), (13), and (14)] and based on supertwist control [Eqs. (8), (9), and (30)] are able to accurately estimate any bounded disturbances. No knowledge about the disturbance mathematical model is required (except for the disturbance boundaries) for the proposed SMDO algorithms to estimate them. Of course, it must be assumed that the bandwidths of the disturbances are much less than the computational frequency of the computer, which implements the SMDO algorithms. The corresponding continuous SMC/SMDO given by Eqs. (8), (19), and (32) accurately addresses the original output tracking problem in the systems (1) and (2) in the presence of bounded disturbances using the control gains that fit the desired compensated dynamics. No high gains, which target the required disturbance attenuation, are used.

There are available methods dedicated to bounded disturbance estimation using neural networks. They provide useful tools for disturbance approximation using a finite set of basis functions with a tuning algorithm that is based on neural networks. This approach [26], developed completely outside of sliding mode framework, minimizes estimation error, but in principle cannot provide its asymptotic convergence to zero. The sliding mode disturbance observers, which are proposed in this paper, are different, much simpler than the neural network estimation algorithm [26] and are able to provide the asymptotic (or even finite time) convergence of the estimation error to zero.

III. Continuous SMC/SMDO for Cascade Systems

Consider a particular nonlinear MIMO system (1) given in quasicascade format

$$\begin{cases} \dot{\boldsymbol{x}}^1 = \boldsymbol{A}^1(\boldsymbol{x}^1)\boldsymbol{x}^2 + \boldsymbol{d}(\boldsymbol{x}^1, \boldsymbol{x}^2, t) \\ \dot{\boldsymbol{x}}^2 = \boldsymbol{A}^2(\boldsymbol{x}^1, \boldsymbol{x}^2) + \boldsymbol{D}(\boldsymbol{x}^1, \boldsymbol{x}^2, t) + \boldsymbol{u} \\ \boldsymbol{y} = \boldsymbol{x}^1 \end{cases} \tag{34}$$

where $\boldsymbol{x}^1, \boldsymbol{x}^2 \in \Re^m$ represent the states, $\boldsymbol{u} \in \Re^m$ is control, $\boldsymbol{A}^1(.) \in \Re^{2\times 2}$, and $\boldsymbol{A}^2(.) \in \Re^2$. The disturbances $\boldsymbol{d}(.) \in \Re^m$ and $\boldsymbol{D}(.) \in \Re^m$ are norm-bounded and $\det[\boldsymbol{A}^1(\boldsymbol{x}^1, \boldsymbol{x}^2)] \neq 0$ in a compact $\boldsymbol{x}^1, \boldsymbol{x}^2 \in \Gamma(\boldsymbol{x}^1, \boldsymbol{x}^2)$.

The asymptotic, decoupled output tracking ($\boldsymbol{y} \to \boldsymbol{y}_c$ as time increases) in the system (34), with unmatched disturbances, is achieved by means of a control design $\boldsymbol{u}$, using the continuous SMC/SMDO technique presented in Sec.II and a backstepping approach [27–29].

The first step is to introduce [in accordance with Eq. (3)] the outer-loop $\boldsymbol{\sigma}^1 \in \Re^m$ and the inner-loop $\boldsymbol{\sigma}^2 \in \Re^m$ sliding variables

$$\begin{aligned} &\boldsymbol{\sigma}^1 = \boldsymbol{e}^1 + \boldsymbol{C}^1\boldsymbol{e}^1_{-1}, \qquad \dot{\boldsymbol{e}}^1_{-1} = \boldsymbol{e}^1, \\ &\boldsymbol{e}^1 = \boldsymbol{x}^1_c = \boldsymbol{x}^1 = \boldsymbol{y}_c - \boldsymbol{x}^1, \qquad \boldsymbol{C}^1 \in R^{m\times m} \end{aligned} \tag{35}$$

$$\begin{aligned} &\boldsymbol{\sigma}^2 = \boldsymbol{e}^2 + \boldsymbol{C}^2\boldsymbol{e}^2_{-1}, \qquad \dot{\boldsymbol{e}}^2_{-1} = \boldsymbol{e}^2, \\ &\boldsymbol{e}^2 = \boldsymbol{x}^2_c - \boldsymbol{x}^2, \qquad \boldsymbol{C}^2 \in R^{m\times m} \end{aligned} \tag{36}$$

where the inner-loop command profile $\boldsymbol{x}^2_c(t)$ and the matrices $\boldsymbol{C}^1$ and $\boldsymbol{C}^2$ are to be identified. The integral terms $\boldsymbol{C}^1\boldsymbol{e}^1_{-1}$ and $\boldsymbol{C}^2\boldsymbol{e}^2_{-1}$ in Eqs. (35) and (36) are added to compensate for the steady-state tracking error in the sliding mode $\boldsymbol{\sigma}^1 = \boldsymbol{\sigma}^2 = \boldsymbol{0}$ due to imperfection of the SMC implementation [26].

Remark 2: Given initial conditions $\boldsymbol{x}^1(0)$ and $\boldsymbol{x}^2(0)$ and, consequently, $\boldsymbol{e}^1(0)$ and $\boldsymbol{e}^2(0)$, the defined initial values

$$\boldsymbol{e}^1_{-1}(0) = -(\boldsymbol{C}^1)^{-1}\boldsymbol{e}^1(0), \qquad \boldsymbol{e}^2_{-1}(0) = -(\boldsymbol{C}^2)^{-1}\boldsymbol{e}^2(0)$$

can avoid reaching phases or can reduce it significantly due to imperfect knowledge of the initial conditions.

Following Eqs. (21) and (33), the desired closed-loop, asymptotically stable dynamics of $\boldsymbol{\sigma}^1$ and $\boldsymbol{\sigma}^2$ are proposed:

$$\begin{cases} \dot{\boldsymbol{\sigma}}^1 = -\boldsymbol{K}^1\boldsymbol{\sigma}^1 + \boldsymbol{A}^1(\boldsymbol{x}^1)\boldsymbol{\sigma}^2 \\ \dot{\boldsymbol{\sigma}}^2 = -\boldsymbol{K}^2\boldsymbol{\sigma}^2 \end{cases} \tag{37}$$

Stability conditions for the system (37) are presented in Theorem 1.

Theorem 1: Assume that

condition a: the matrix $\boldsymbol{A}^1(\boldsymbol{x}^1)$ is norm-bounded, that is,

$$\|\boldsymbol{A}^1(\boldsymbol{x}^1)\| \le M$$

condition b:

$$\begin{aligned} &\boldsymbol{K}^1 = diag\{K^1_i\}, \qquad \boldsymbol{K}^2 = diag\{K^2_i\}, \\ &K^j_i > 0 \quad \forall\ i = 1, \ldots, m \quad \forall\ j = 1, 2 \end{aligned}$$

condition c:

$$\lambda_{\min}(\boldsymbol{K}^1) \cdot \lambda_{\min}(\boldsymbol{K}^2) > M^2/4$$

where $\lambda_{\min}(\boldsymbol{K}^j)$ is a minimal eigenvalue of the matrix $\boldsymbol{K}^j \quad \forall\ j = 1, 2$, then the origin of the system (37) is globally asymptotically stable.

Proof: Consider a Lyapunov function given by

$$V = \tfrac{1}{2}(\boldsymbol{\sigma}^1)^T\boldsymbol{\sigma}^1 + \tfrac{1}{2}(\boldsymbol{\sigma}^2)\boldsymbol{\sigma}^2 > 0 \quad \forall\ \boldsymbol{\sigma}^1, \qquad \boldsymbol{\sigma}^2 \neq 0$$

and compute its derivative on the trajectory of the system (37):

$$\begin{aligned} \dot{V} &= (\boldsymbol{\sigma}^1)^T[-\boldsymbol{K}^1\boldsymbol{\sigma}^1 + \boldsymbol{A}^1(\boldsymbol{x}^1)\boldsymbol{\sigma}^2] - (\boldsymbol{\sigma}^2)^T\boldsymbol{K}^2\boldsymbol{\sigma}^2 \\ &\le -\lambda_{\min}(\boldsymbol{K}^1)\|\boldsymbol{\sigma}^1\|^2 - \lambda_{\min}(\boldsymbol{K}^2)\|\boldsymbol{\sigma}^2\|^2 + M\|\boldsymbol{\sigma}^1\| \cdot \|\boldsymbol{\sigma}^2\| \\ &= -\left(\sqrt{\lambda_{\min}(\boldsymbol{K}^1)}\|\boldsymbol{\sigma}^1\| - \sqrt{\lambda_{\min}(\boldsymbol{K}^2)}\|\boldsymbol{\sigma}^2\|\right)^2 \\ &\quad - \left(2\sqrt{\lambda_{\min}(\boldsymbol{K}^1) \cdot \lambda_{\min}(\boldsymbol{K}^2)} - M\right)\|\boldsymbol{\sigma}^1\| \cdot \|\boldsymbol{\sigma}^2\| \end{aligned}$$

Then $\dot{V} < 0$ if the condition c holds, and the theorem is proven.

Remark 3: The continuous SMC/SMDO control $\boldsymbol{u}$ in system (34) is designed to robustly enforce the sliding variable dynamics given by system (37) in the presence of bounded disturbances $\boldsymbol{d}(\boldsymbol{x}^1, \boldsymbol{x}^2, t)$ and $\boldsymbol{D}(\boldsymbol{x}^1, \boldsymbol{x}^2, t)$. Selecting

$$K^2_i \gg K^1_i \quad \forall\ i = 1, \ldots, m$$

(time scale) will provide for faster asymptotic convergence of the inner-loop sliding variable $\boldsymbol{\sigma}^2 \to 0$ and slower convergence of the outer-loop sliding variable $\boldsymbol{\sigma}^1 \to 0$ as time increases. This yields decoupling of inner- and outer-loop sliding variable dynamics, which can be useful in implementing the algorithms. Note that time-scale separation recommended in previous SMC implementations [10,11], between the inner and outer-loop output tracking error dynamics in the sliding mode $\boldsymbol{\sigma}^1 = \boldsymbol{\sigma}^2 = \boldsymbol{0}$, is not required based on the presented stability analysis.

The second step is to identify the inner-loop command profile $\boldsymbol{x}^2_c$. Differentiating Eq. (35) and equating the right-hand sides of this derivative and the first equation in system (37), we obtain

$$\boldsymbol{x}^2_c = [\boldsymbol{A}^1(\boldsymbol{x}^1)]^{-1}(\bar{\boldsymbol{d}} + \boldsymbol{C}^1\boldsymbol{e}^1 + \boldsymbol{K}^1\boldsymbol{\sigma}^1) - \boldsymbol{C}^2\boldsymbol{e}^2_{-1} \tag{38}$$

where $\bar{\boldsymbol{d}} = \dot{\boldsymbol{y}}_c - \boldsymbol{d}(.)$.

In the third step, we identify the continuous control law $\boldsymbol{u}$ that provides asymptotic output tracking in the quasicascade nonlinear system (34) with bounded, unmatched disturbances. Differentiating Eq. (36) and equating the right-hand sides of this derivative and the second equation in system (37), we obtain

$$\boldsymbol{u} = \bar{\boldsymbol{D}} + \boldsymbol{A}^2(\boldsymbol{x}^1, \boldsymbol{x}^2) + \boldsymbol{C}^2\boldsymbol{e}^2 + \boldsymbol{K}^2\boldsymbol{\sigma}^2 \tag{39}$$

where $\bar{\boldsymbol{D}} = \dot{\boldsymbol{x}}_c^2 - \boldsymbol{D}(.)$.

Because the bounded disturbances $\bar{\boldsymbol{d}}$ and $\bar{\boldsymbol{D}}$ are not known, they must be estimated with an SMDO in order to implement the control laws (38) and (39).

In the final step of the controller design, the SMDO is designed to estimate bounded disturbances $\bar{\boldsymbol{d}}$ and $\bar{\boldsymbol{D}}$. Either of the two algorithms studied in Sec. II can be employed. The first SMDO algorithm is based on traditional SMC in accordance with Eqs. (8–10), (13), and (14). The second one is based on supertwisting HOSM in accordance with Eqs. (8), (9), and (30).

Enforcement of the sliding variable dynamics [system_(37)] with the SMC/SMDO design [control laws (38) and (39)] (taking into account the dynamics of the SMDO) is summarized in the following theorem.

Theorem 2: Assuming the conditions_a, b, and c of Theorem 1 are met, then the sliding variables will tend to zero, that is, $\boldsymbol{\sigma}^1, \boldsymbol{\sigma}^2 \to 0$, as time increases if the disturbances $\bar{\boldsymbol{d}}$ and $\bar{\boldsymbol{D}}$ in system (34) are estimated via an SMDO based on supertwisting SMC. If the disturbances $\bar{\boldsymbol{d}}$ and $\bar{\boldsymbol{D}}$ in system–(34) are estimated via an SMDO based on traditional SMC, then $\boldsymbol{\sigma}^1, \boldsymbol{\sigma}^2 \to \Omega$, where

$$\Omega\colon \left\{\boldsymbol{\sigma}^1, \boldsymbol{\sigma}^2\colon \frac{\mathcal{O}(\tau_1)}{\|\boldsymbol{\sigma}^2\|} + \frac{\mathcal{O}(\tau_2)}{\|\boldsymbol{\sigma}^1\|} \geq 2\sqrt{\lambda_{\min}(\boldsymbol{K}^1)\cdot\lambda_{\min}(\boldsymbol{K}^2)} - M\right\}$$

is a domain of asymptotic convergence.

Proof: The SMDO based on supertwisting SMC, and designed similarly to Eqs. (9), (30), and (31), estimates the bounded disturbances $\bar{\boldsymbol{d}}$ and $\bar{\boldsymbol{D}}$ in system (34) in finite time. Therefore, as soon as the estimation error converges to zero, the sliding variable dynamics are described by system (37), and $\boldsymbol{\sigma}^1, \boldsymbol{\sigma}^2 \to \boldsymbol{0}$ asymptotically in accordance with Theorem 1.

The SMDO based on traditional SMC and designed similarly to Eqs. (9–14) and (18) estimates the bounded disturbances $\bar{\boldsymbol{d}}$ and $\bar{\boldsymbol{D}}$ in system (34) asymptotically. The estimation errors, $\bar{\boldsymbol{d}} - \hat{\bar{\boldsymbol{d}}}$ and $\bar{\boldsymbol{D}} - \hat{\bar{\boldsymbol{D}}}$, converge asymptotically to the domains, $\mathcal{O}(\tau_1)$ and $\mathcal{O}(\tau_2)$, where τ_1 and τ_2 correspond to LPF time constants, that is,

$$\|\bar{\boldsymbol{d}} - \hat{\bar{\boldsymbol{d}}}\| \to \mathcal{O}(\bar{\tau}_1), \qquad \|\bar{\boldsymbol{D}} - \hat{\bar{\boldsymbol{D}}}\| \to \mathcal{O}(\bar{\tau}_2)$$

in Sec. II). Assume that the SMDO asymptotic dynamics for estimating the disturbances $\bar{\boldsymbol{d}}$ and $\bar{\boldsymbol{D}}$ are given as

$$\bar{\tau}_1\dot{\hat{\bar{\boldsymbol{d}}}} = -\hat{\bar{\boldsymbol{d}}} + \bar{\boldsymbol{d}}, \qquad \bar{\tau}_2\dot{\hat{\bar{\boldsymbol{D}}}} = -\hat{\bar{\boldsymbol{D}}} + \bar{\boldsymbol{D}} \tag{40}$$

Then the actual sliding variables $\boldsymbol{\sigma}^1$ and $\boldsymbol{\sigma}^2$ closed-loop dynamics are derived, taking into account Eqs. (35), (36), and (38–40):

$$\begin{cases} \dot{\boldsymbol{\sigma}}^1 = \bar{\boldsymbol{d}} - \hat{\bar{\boldsymbol{d}}} - \boldsymbol{K}^1\boldsymbol{\sigma}^1 + \boldsymbol{A}(\boldsymbol{x}^1)\boldsymbol{\sigma}^2 \\ \dot{\boldsymbol{\sigma}}^2 = \bar{\boldsymbol{D}} - \hat{\bar{\boldsymbol{D}}} - \boldsymbol{K}^2\boldsymbol{\sigma}^2 \end{cases} \tag{41}$$

Now, consider a Lyapunov function given by

$$V = \tfrac{1}{2}(\boldsymbol{\sigma}^1)^T\boldsymbol{\sigma}^1 + \tfrac{1}{2}(\boldsymbol{\sigma}^2)\boldsymbol{\sigma}^2 > 0 \quad \forall\ \boldsymbol{\sigma}^1, \boldsymbol{\sigma}^2 \neq 0$$

and compute its derivative on the trajectory of the system (41):

$$\begin{aligned} \dot{V} &= (\boldsymbol{\sigma}^1)^T[-\boldsymbol{K}^1\boldsymbol{\sigma}^1 + \boldsymbol{A}^1(\boldsymbol{x}^1)\boldsymbol{\sigma}^2 + \bar{\boldsymbol{d}} - \hat{\bar{\boldsymbol{d}}}] \\ &\quad + (\boldsymbol{\sigma}^2)^T[-\boldsymbol{K}^2\boldsymbol{\sigma}^2 + \bar{\boldsymbol{D}} - \hat{\bar{\boldsymbol{D}}}] \leq -\lambda_{\min}(\boldsymbol{K}^1)\|\boldsymbol{\sigma}^1\|^2 \\ &\quad - \lambda_{\min}(\boldsymbol{K}^2)\|\boldsymbol{\sigma}^2\|^2 + M\|\boldsymbol{\sigma}^1\|\cdot\|\boldsymbol{\sigma}^2\| + \mathcal{O}(\tau_1)\|\boldsymbol{\sigma}^1\| + \mathcal{O}(\tau_2)\|\boldsymbol{\sigma}^2\| \\ &= -\left(\sqrt{\lambda_{\min}(\boldsymbol{K}^1)}\|\boldsymbol{\sigma}^1\| - \sqrt{\lambda_{\min}(\boldsymbol{K}^2)}\|\boldsymbol{\sigma}^2\|\right)^2 \\ &\quad - \left(2\sqrt{\lambda_{\min}(\boldsymbol{K}^1)\cdot\lambda_{\min}(\boldsymbol{K}^2)} - M - \frac{\mathcal{O}(\tau_1)}{\|\boldsymbol{\sigma}^2\|} - \frac{\mathcal{O}(\tau_2)}{\|\boldsymbol{\sigma}^1\|}\right)\|\boldsymbol{\sigma}^1\|\cdot\|\boldsymbol{\sigma}^2\| \end{aligned}$$

It is apparent that a domain of asymptotic convergence can be defined as

$$\Omega\colon \left\{\boldsymbol{\sigma}^1, \boldsymbol{\sigma}^2\colon \frac{\mathcal{O}(\tau_1)}{\|\boldsymbol{\sigma}^2\|} + \frac{\mathcal{O}(\tau_2)}{\|\boldsymbol{\sigma}^1\|} \geq 2\sqrt{\lambda_{\min}(\boldsymbol{K}^1)\cdot\lambda_{\min}(\boldsymbol{K}^2)} - M\right\}$$

This concludes the proof of Theorem 2.

IV. RLV Mathematical Model

The nonlinear Newton–Euler equations of motion for the rigid vehicle were chosen for the RLV flight control system design. The rotational equations of motion, using notation from Wise and Broy [30], are

$$\begin{aligned} \dot{p} &= -L_{pq}pq - L_{qr}qr + L + f_L, \\ \dot{q} &= -M_{pr}pr - M_{r^2p^2}(r^2 - p^2) + M + f_M, \\ \dot{r} &= -N_{pq}pq - N_{qr}qr + N + f_N \end{aligned} \tag{42}$$

In Eq. (42), p, q, and r are roll, pitch, and yaw rates, respectively; $L_{pq}, L_{qr}, M_{pr}, M_{r^2p^2}, N_{pq}$, and N_{qr} are functions of vehicle inertia; L, M, and N are roll, pitch, and yaw accelerations arising from aerodynamics; and f_L, f_M, and f_N are disturbance accelerations. Translational accelerations $(\dot{u}, \dot{v}, \dot{w})$ in the vehicle body frame are

$$\begin{aligned} \dot{u} &= rv - qw + X + G_x\dot{v} \\ &= pw - ru + Y + G_y\dot{w} \\ &= qu - pv + Z + G_z \end{aligned} \tag{43}$$

The accelerations X, Y, and Z in Eq. (43) are from aerodynamics, and G_x, G_y, and G_z are gravity terms given by

$$\begin{aligned} &G_x = -g\sin(\theta), \qquad G_y = g\cos(\theta)\sin(\phi), \\ &G_z = g\cos(\theta)\cos(\phi) \end{aligned} \tag{44}$$

The Euler angles that define the orientation of the vehicle relative to an inertial frame are

$$\begin{bmatrix} \dot{\phi} \\ \dot{\theta} \\ \dot{\psi} \end{bmatrix} = \begin{bmatrix} 1 & \tan\theta\sin\phi & \tan\theta\cos\phi \\ 0 & \cos\phi & -\sin\phi \\ 0 & \frac{\sin\phi}{\cos\theta} & \frac{\cos\phi}{\cos\theta} \end{bmatrix}\begin{bmatrix} p \\ q \\ r \end{bmatrix} \tag{45}$$

In Eq. (45), ϕ is the roll angle, θ is the pitch angle, and ψ is the yaw angle. Aerodynamic surfaces for the RLV are represented by three virtual surfaces (aileron, elevator, and rudder). Commanded virtual deflections

$$\boldsymbol{\delta}_c = \{\delta_{ac}, \delta_{ec}, \delta_{rc}\} \in \Re^3$$

(the subscripts a, e, and r represent aileron, elevator, and rudder, respectively) are distributed by a control allocator to actual aerosurface actuator commands:

$$\bar{\boldsymbol{\delta}}_c = \{\delta_{elc}, \delta_{erc}, \delta_{flc}, \delta_{frc}, \delta_{rlc}, \delta_{rrc}\} \in \Re^6$$

where the subscripts el, er, fl, fr, rl, and rr represent left and right elevons, left and right flaps, and left and right rudders, respectively.

These commands are sent to the individual aerosurface actuators modeled here by first-order systems:

$$\tau_i \dot{\delta}_i = \delta_{ic} - \delta_i \tag{46}$$

where $i = el, er, fl, fr, rl$, and rr.

The actual deflection angles in Eq. (46) are δ_i, the actuator time constants are τ_i, and the actuator command inputs are δ_{ic}.

Remark 4: The aerosurface actuator models in Eq. (46) are simplifications of the actual models, which are of higher order and nonlinear. Modeling them as simple, linear first order as in Eq. (46) simplifies the controller design. In the simulations used to verify the design, the actuators were modeled as second-order systems with the following position and rate limits:

$$-30\,\text{deg} \le \delta_i \le 25\,\text{deg}, \qquad |\dot{\delta}_i| \le 30\ \text{deg/s}$$

where $i = el, er$

$$-15\,\text{deg} \le \delta_j \le 26\,\text{deg}, \qquad |\dot{\delta}_j| \le 10\ \text{deg/s}$$

where $j = fl, fr$

$$-30\,\text{deg} \le \delta_{rl} \le 60\,\text{deg}, \qquad |\dot{\delta}_{rl}| \le 30\ \text{deg/s}$$

$$-60\,\text{deg} \le \delta_{rr} \le 30\,\text{deg}, \qquad |\dot{\delta}_{rr}| \le 30\ \text{deg/s}$$

V. RLV Control Problem Formulation

The general problem for the flight control system during TAL is to determine aerosurface deflection commands such that the guidance commands are robustly, asymptotically followed in the presence of external disturbances and uncertainties in the plant. Guidance commands in the TAL flight are N_{zc} normal acceleration (or $A_z = -N_{zc}$, body frame acceleration command), ϕ_c roll angle, and r_c yaw rate.

To use the control algorithm developed in Secs. II and III for the RLV controller design, the RLV mathematical model [Eqs. (42–46)] is presented in a format given by system (34), where $x^1 = \{A_z, \varphi\}^T$ and $x^2 = \{p, q\}^T$:

$$\begin{cases} \begin{bmatrix} \dot{A}_z \\ \dot{\phi} \end{bmatrix} = \begin{bmatrix} \dot{v} & -\dot{u} \\ 1 & \tan\theta \sin\phi \end{bmatrix} \begin{bmatrix} p \\ q \end{bmatrix} + \begin{bmatrix} f_{Az} \\ f_\phi \end{bmatrix} \\ \begin{bmatrix} \dot{p} \\ \dot{q} \end{bmatrix} = \begin{bmatrix} -L_{pq} pq - L_{qr} qr \\ -M_{pr} pr - M_{r^2p^2}(r^2 - p^2) \end{bmatrix} + \begin{bmatrix} L \\ M \end{bmatrix} + \begin{bmatrix} f_L \\ f_M \end{bmatrix} \\ \dot{r} = -N_{pq} pq - N_{qr} qr + N + f_N \end{cases} \tag{47}$$

where $\boldsymbol{d} = \{f_{Az}, f_\phi\}^T$ is a disturbance vector in the normal acceleration and roll channels (f_ϕ is caused by modeling errors, whereas f_{Az} comprises modeling errors and external disturbances), $\boldsymbol{D} = \{f_L, f_M\}^T$ is a disturbance vector in the roll rate and the pitch rate channels, and f_N is a disturbance in the yaw rate channel. All disturbances are bounded in a reasonable flight domain.

The goal is to design a continuous SMC/SMDO controller that provides decoupled asymptotic output tracking, that is, $A_z \to A_{zc}$, $\varphi \to \varphi_c$, and $r \to r_c$ as time increases, in the presence of bounded disturbances d, D, and f_N by means of roll, pitch, and yaw acceleration commands L_c, M_c, and N_c.

Remark 5: It is essential for the controller design that the matrix

$$\boldsymbol{A}^1 = \begin{bmatrix} \dot{v} & -\dot{u} \\ 1 & \tan\theta \sin\phi \end{bmatrix} \tag{48}$$

should be nonsingular in a reasonable operational domain. Simulations of the RLV confirm that it is. Linear accelerations $\dot{v}$ and $\dot{u}$, pitch θ, and roll φ angles are assumed to be measured or computed based on the other available measurements. The determinant of $\boldsymbol{A}^1$ for a typical TAEM trajectory is shown in Fig. 2. Except for initiation of TAEM control, this quantity is nonzero for all of flight. In application, det $\boldsymbol{A}^1$ would be initialized to a suitable nonzero value. The RLV, in the flight regime studied, is always in accelerated flight. Although $\dot{v}$ may get very small, $\dot{u}$ and, likewise, drag force are always present. That is why det $\boldsymbol{A}^1 \neq 0$. Using this matrix would have to be reconsidered for RLV flight control in another flight regime. As discussed in Sec. VII, however, $\boldsymbol{A}^1$ is replaced with

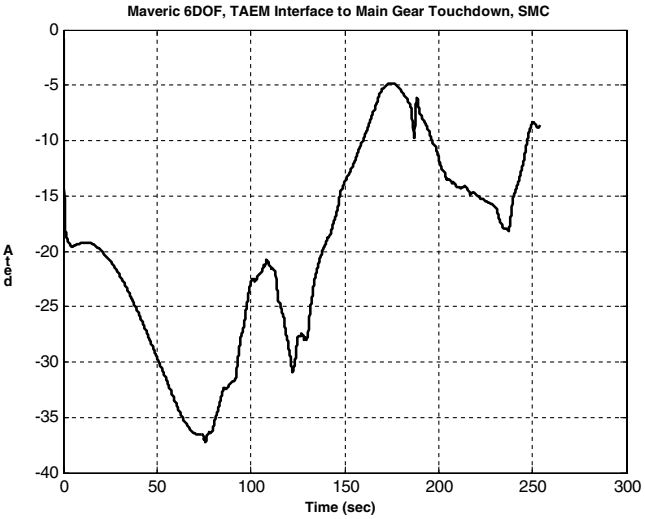

Fig. 2 Determinant A^1 for a typical trajectory.

$$\boldsymbol{A}^1 = \begin{bmatrix} 1 & 0 \\ 0 & 1 \end{bmatrix}$$

for a preliminary controller design without compromising performance or robustness.

The control problem is addressed using the continuous SMC/SMDO algorithm presented in Secs. II and III, in the following steps:

1) A control law for the outer loop is designed in terms of virtual rate commands p_c and q_c.

2) A control law for the inner loop is designed in terms of angular accelerations L_c and M_c.

3) A control law for the yaw rate channel is designed in terms of angular acceleration N_c.

4) A control allocation matrix $\boldsymbol{B}_A$ is used to map the angular acceleration command vector to the actuator virtual deflection commands:

$$\boldsymbol{\delta}_c = \boldsymbol{B}_A \boldsymbol{I} \begin{bmatrix} L_c \\ M_c \\ N_c \end{bmatrix}, \qquad \boldsymbol{\delta}_c = \{\delta_{ac}, \delta_{ec}, \delta_{rc}\} \Re^3, \qquad \boldsymbol{B}_A \Re^{3\times 3} \tag{49}$$

where $\boldsymbol{I} \in \Re^{3x3}$ is a constant inertia matrix.

A control allocator is then used to distribute the virtual actuator commands $\boldsymbol{\delta}_c$ to actual aerosurface actuator commands $\bar{\boldsymbol{\delta}}_c$, which are fed to the individual actuators [Eq. (46)], that is,

$$\bar{\boldsymbol{\delta}}_c = CA(\delta_c), \qquad \bar{\boldsymbol{\delta}}_c = \{\delta_{elc}, \delta_{erc}, \delta_{flc}, \delta_{frc}, \delta_{rlc}, \delta_{rrc}\} \Re^6 \tag{50}$$

The desired RLV performance criterion is to robustly track the guidance command profiles N_{zc}, ϕ_c, and r_c, such that the compensated dynamics for each tracking error is described by linear, decoupled, homogeneous differential equations with the desired time-scale separation and eigenvalue placement as in Eqs. (35–37).

VI. RLV Multiple-Loop Continuous SMC/SMDO Design

Tracking of the commanded guidance profiles is achieved through a two-loop SMC structure. Its functional diagram is presented in Fig. 3.

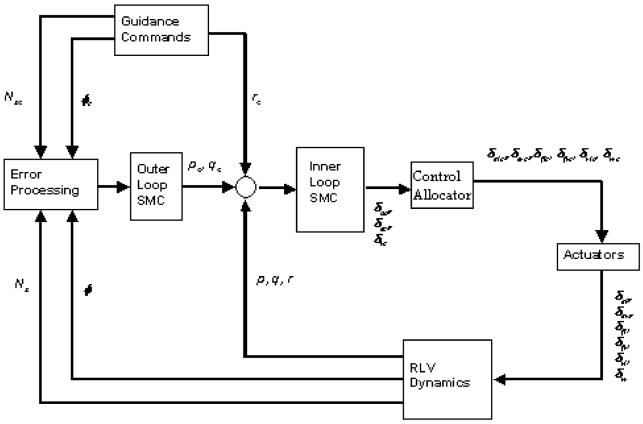

Fig. 3 Multiple-loop SMDO-driven SMC functional diagram.

The cascade structure of the RLV dynamics [Eq. (47)] is exploited in the design of a two-loop flight control system using continuous SMC/SMDO. Together, the two loops provide decoupled, asymptotic tracking of the guidance profiles in the presence of bounded external disturbances and plant uncertainties

A. Outer-Loop Controller Design

The outer-loop SMC takes the guidance commands for normal acceleration N_{zc} and roll angle ϕ_c, and produces roll and pitch virtual rate commands $p_c$and q_c to the inner loop. A normal acceleration command is first converted to a body frame acceleration command A_{zc}, simply by negating it. The outer-loop input-output dynamics are taken as the upper part of Eq. (47)

$$\begin{bmatrix} \dot{A}_z \\ \dot{\phi} \end{bmatrix} = \begin{bmatrix} \dot{v} & -\dot{u} \\ 1 & \tan\theta \sin\phi \end{bmatrix} \begin{bmatrix} p \\ q \end{bmatrix} + \begin{bmatrix} f_{Az} \\ f_{\phi} \end{bmatrix} \tag{51}$$

where $|f_{Az}| \le L_{Az}$ and $|f_{\phi}| \le L_{\phi}$ are disturbances (bounded in a reasonable flight envelope) in normal acceleration and roll channels, respectively, and $\dot{v}$ and $\dot{u}$ are measured or calculated.

The problem is to design continuous virtual controls p_c and q_c that asymptotically follow the reference profiles A_{zc} and ϕ_c in system (51) in the presence of bounded disturbances f_{Az} and f_{ϕ}.

Following the continuous SMC/SMDO controller design algorithm presented in Secs. II and III, the components of the vector sliding variable $\{\sigma_{Az}, \sigma_{\phi}\}^T$ are introduced as in Eq. (3):

$$\sigma_i = e_i + c_i e_{i-1}, \qquad \dot{e}_{i-1} = e_i \tag{52}$$

with $i = A_z, \phi$ and

$$e_{Az} = A_{zc} - A_z, \qquad e_{\phi} = \phi_c - \phi \tag{53}$$

In the sliding mode $\sigma_{Az} = \sigma_{\phi} = \mathbf{0}$, the outer-loop compensated error dynamics are decoupled in accordance with Eqs. (35) and (52). The gains $c_{Az} > 0$ and $c_{\phi} > 0$ are chosen such that the tracking errors e_{Az} and e_{ϕ} exhibit the desired linear asymptotic behavior in the sliding modes $\sigma_{Az} = 0$ and $\sigma_{\phi} = 0$. Now, the objective of the outer loop is to generate continuous virtual controls p_c and q_c and to provide asymptotic convergence of the system (51) to the sliding surface (52) $\sigma_{Az}, \sigma_{\phi} \to 0$. The virtual controls p_c and q_c are designed in the following way:

$$\begin{bmatrix} p_c \\ q_c \end{bmatrix} = \begin{bmatrix} \dot{v} & -\dot{u} \\ 1 & \tan\theta \sin\phi \end{bmatrix}^{-1} \begin{bmatrix} \hat{d}_{Az} + c_{Az} e_{Az} + K_{Az} \sigma_{Az} \\ \hat{d}_{\phi} + c_{\phi} e_{\phi} + K_{\phi} \sigma_{\phi} \end{bmatrix} - \begin{bmatrix} c_L & 0 \\ 0 & c_M \end{bmatrix} \begin{bmatrix} e_{L-1} \\ e_{M-1} \end{bmatrix} \tag{54}$$

where $\hat{d}_{Az}$ is an estimate of $d_{Az} = \dot{A}_{Azc} - f_{Az}$ and $\hat{d}_{\phi}$ is an estimate of $d_{\phi} = \ddot{\varphi}_{Ac} - f_{\phi}$. These estimates are to be obtained by an SMDO with gain adaptation based on traditional SMC in Eqs. (8), (9), (13), and (14). The last term in Eq. (54),

$$\begin{bmatrix} c_L & 0 \\ 0 & c_M \end{bmatrix} \begin{bmatrix} e_{L-1} \\ e_{M-1} \end{bmatrix}$$

will be defined in Sec. VI.B.

Assuming

$$|d_{Az}| \le \bar{L}_{Az}, \qquad |d_{\phi}| \le \bar{L}_{\phi}$$

in a reasonable flight envelope, and denoting

$$\begin{bmatrix} \lambda_{Az} \\ \lambda_{\phi} \end{bmatrix} = \begin{bmatrix} \dot{v} & -\dot{u} \\ 1 & \tan\theta \sin\phi \end{bmatrix} \begin{bmatrix} p \\ q \end{bmatrix}$$

the adaptive-gain SMDO based on traditional SMC is designed in accordance with Eqs. (8–14),

1) The components of the auxiliary vector-sliding variable $\{s_{Az}, s_{\phi}\}^T$ are introduced in accordance with Eq. (8):

$$s_i = \sigma_i + z_i, \qquad \dot{z}_i = \lambda_i - c_i e_i - v_i, \qquad i = A_z, \phi \tag{55}$$

The auxiliary vector-sliding variable dynamics are derived:

$$\dot{s}_i = d_i - v_i, \quad i = A_z, \phi \tag{56}$$

2) Using the Lyapunov function technique, as in Eqs. (9–12), it is easy to show that the SMC auxiliary control functions

$$v_i = (\bar{L}_i + \rho_i)\text{sign}(\sigma_i) \tag{57}$$

with $i = A_z, \phi$, stabilize the auxiliary sliding variables s_{Az} and s_{ϕ} at zero in the finite times

$$t_i \le \frac{|\sigma_i(\mathbf{0})|}{\rho_i}$$

and $i = A_z, \phi$, respectively. Therefore, the equivalent auxiliary control functions v_{Azeq} and $v_{\phi eq}$ exactly estimate the disturbances

$$d_{Az} \quad \forall\ t > t_{Az}, \qquad d_{\phi} \quad \forall\ t > t_{\phi}$$

To estimate auxiliary equivalent controls v_{Azeq} and $v_{\phi eq}$, the SMC control function [Eq. (57)] is to be low-pass filtered as in Eq. (14) with $i = Az, \phi$. To reduce the high-frequency switching amplitudes in Eq. (57), the gain-adaptation algorithm presented in Sec. II is used

$$v_i = \begin{cases} (\bar{L}_i + \rho_i)\text{sign}(s_i), & \text{if } |s_i| > \mu_i \\ (|\hat{v}_{ieq}| + \rho_i)\text{sign}(s_i), & \text{if } |s_i| \le \mu_i \end{cases} \tag{58}$$

where $\mu_i \sim \Delta T$ (computer time increment) and $i = Az, \phi$. The design of the outer-loop virtual controller [Eq. (54)] is completed after substitution of the disturbance estimates $\hat{d}_{Az} = \hat{v}_{Azeq}$ and $\hat{d}_{\phi} = \hat{v}_{\phi eq}$. The functions $\hat{v}_{Azeq}$ and $\hat{v}_{\phi eq}$ are computed using an adaptive-gain SMDO in Eqs. (14), (55), (56), and (58).

B. Inner-Loop SMC Design

The inner-loop SMC takes the body rate virtual control commands $p_c$and q_c, generated by the outer-loop controller [Eqs. (54) and (58)], and the yaw rate command r_c that comes from the guidance function. To provide turn coordination, a stability augmentation system style yaw rate command was generated. Using the fact that for a given bank angle and true air speed there is only one yaw rate for which turn coordination can be achieved, the stability augmentation system yaw rate command can be derived [31]:

$$r_{c\text{SAS}} = (g/U)\sin\phi \tag{59}$$

The error signal used in the yaw rate loop SMC is

$$e_{\text{SAS}} = (r_c + r_{c\text{SAS}} - r) \tag{60}$$

The inner-loop continuous SMC/SMDO controller is supposed to follow the body rate virtual control commands in the presence of bounded disturbances f_L, f_M, and f_N by generating pitch, roll, and

yaw acceleration commands L_c, M_c, and N_c. In addition to tracking virtual body rate commands, the inner loop causes the system to exhibit linear decoupled motion in sliding mode. No time scale (separation) between the inner and outer-loop compensated dynamics is required. The inner-loop input-output dynamics are taken as the lower part of Eq. (47):

$$\begin{bmatrix} \dot{p} \\ \dot{q} \\ \dot{r} \end{bmatrix} = \begin{bmatrix} -L_{pq}pq - L_{qr}qr \\ -M_{pr}pr - M_{r^2p^2}(r^2 - p^2) \\ -N_{pq}pq - N_{qr}qr \end{bmatrix} + \begin{bmatrix} L \\ M \\ N \end{bmatrix} + \begin{bmatrix} f_L \\ f_M \\ f_N \end{bmatrix} \tag{61}$$

where f_L, f_M, and f_N are bounded disturbances (in a reasonable flight envelope) in roll, pitch, and yaw channels, respectively.

Following the continuous SMC/SMDO controller design algorithm presented in Secs. II and III, the components of the vector-sliding variable $\{\sigma_L, \sigma_M, \sigma_N\}^T$ are introduced, as in Eq. (52), with $i = L, M, N$ and

$$e_L = p_c - p, \qquad e_M = q_c - q, \qquad e_N = e_{\text{SAS}} \tag{62}$$

In the sliding mode $\sigma_L = \sigma_M = \sigma_N = 0$, the inner-loop compensated error dynamics are decoupled in accordance with Eqs. (36) and (62). The gains $c_L > 0$, $c_M > 0$, and $c_N > 0$ are chosen such that the tracking errors e_L, e_M, and e_N exhibit the desired linear asymptotic behavior in the sliding mode $\sigma_L = \sigma_M = \sigma_N = 0$. The objective of the inner loop is to generate continuous controls L_c, M_c, and N_c, that provide asymptotic convergence of the system (61) to the sliding surfaces (52) and (62) and $\sigma_L = \sigma_M = \sigma_N = 0$. The pitch, roll, and yaw acceleration control commands, L_c, M_c, and N_c, are designed in a format

$$\begin{bmatrix} L_c \\ M_c \\ N_c \end{bmatrix} = \begin{bmatrix} \hat{\bar{f}}_L \\ \hat{\bar{f}}_M \\ \hat{\bar{f}}_N \end{bmatrix} \begin{bmatrix} -L_{pq}pq - L_{qr}qr \\ -M_{pr}pr - M_{r^2p^2}(r^2 - p^2) \\ -N_{pq}pq - N_{qr}qr \end{bmatrix} + \begin{bmatrix} c_L & 0 & 0 \\ 0 & c_M & 0 \\ 0 & 0 & c_N \end{bmatrix} \begin{bmatrix} e_L \\ e_M \\ e_N \end{bmatrix} + \begin{bmatrix} K_L & 0 & 0 \\ 0 & K_M & 0 \\ 0 & 0 & K_N \end{bmatrix} \begin{bmatrix} \sigma_L \\ \sigma_M \\ \sigma_N \end{bmatrix} \tag{63}$$

where

$$\begin{bmatrix} \hat{\bar{f}}_L \\ \hat{\bar{f}}_M \\ \hat{\bar{f}}_N \end{bmatrix}$$

is the estimate for the bounded accumulated disturbance

$$\begin{bmatrix} \bar{f}_L \\ \bar{f}_M \\ \bar{f}_N \end{bmatrix} = \begin{bmatrix} \dot{p}_c - f_L \\ \dot{q}_c - f_M \\ \dot{r}_c - f_N \end{bmatrix}$$

Assuming

$$|\bar{f}_L| \le \bar{L}_L, \qquad |\bar{f}_M| \le \bar{L}_M, \qquad |\bar{f}_N| \le \bar{L}_N$$

in a reasonable flight envelope, the adaptive-gain SMDO based on traditional SMC is designed in accordance with Eqs. (8–14) as follows:

1) The components of the auxiliary vector-sliding variable $\{s_L, s_M, s_N\}^T$ are introduced as in Eq. (55)

$$s_i = \sigma_i + z_i, \qquad \dot{z}_i = \lambda_i - c_i e_i - v_i, \qquad i = L, M, N, \qquad \lambda_i = i \tag{64}$$

and the auxiliary vector-sliding variable dynamics are derived as in Eq. (56)

$$\dot{s}_i = \bar{f}_i - v_i, \qquad i = L, M, N \tag{65}$$

2) The auxiliary SMC control functions v_L, v_M, and v_N are defined as in Eq. (57) with $i = L, M$, and N and stabilize the auxiliary sliding variables s_L, s_M, and s_N to zero in the finite times

$$t_i \le \frac{|\sigma_i(\mathbf{0})|}{\rho_i}$$

with $i = L$, M, and N, respectively. Therefore, the equivalent auxiliary control functions v_L, v_M, and v_N estimate exactly the disturbances

$$\bar{f}_L \quad \forall\ t > t_L, \qquad \bar{f}_M \quad \forall\ t > t_M, \qquad \bar{f}_N \quad \forall\ t > t_N$$

3) The equivalent controls $v_{L\text{eq}}$, $v_{M\text{eq}}$, and $v_{N\text{eq}}$ from the low-pass filter are defined as in Eq. (14) with $i = L$, M, and N. The gain-adaptation algorithm is taken as in Eq. (58) with $i = L$, M, and N.

The design of the inner-loop controller [Eq. (63)] is completed after substitution of the disturbance estimates

$$\hat{\bar{f}}_L = \hat{v}_{L\text{eq}}, \qquad \hat{\bar{f}}_M = \hat{v}_{M\text{eq}}, \qquad \hat{\bar{f}}_N = \hat{v}_{N\text{eq}}$$

where $\hat{v}_{L\text{eq}}$, $\hat{v}_{M\text{eq}}$, and $\hat{v}_{N\text{eq}}$ are computed using an adaptive-gain SMDO as in Eqs. (14), (57), (58), (64), and (65) with $i = L$, M, and N.

C. Assessment of Double-Loop RLV Control System Stability

Given in Sec. VI, stability analysis of a generalized quasicascade system controlled via time-scaled SMC/SMDO in system (34) is valid for the RLV control system in Eqs. (47), (54), and (63) because the later falls into a class of quasicascade systems (34). The effect of cascaded, second-order unmodeled dynamics on the performance of the SMC/SMDO is analyzed in Sec. II [Eqs. (25–28)]. There is significant room for tuning the controller for the RLV with unmodeled dynamics, including actuator dynamics [Eq. (46)], while retaining overall control system stability.

Sliding variables σ_{Az}, σ_ϕ, σ_L, σ_M, and σ_N compensated dynamics are derived by differentiating Eqs. (52) and (62) and substituting controls (54) and (63). Assuming that the first-order lag blocks describe the SMDO dynamics as soon as the auxiliary sliding variables are reached, then the sliding variable compensated dynamics are presented as

$$\begin{bmatrix} \dot{\sigma}_{Az} \\ \dot{\sigma}_\phi \end{bmatrix} = \begin{bmatrix} d_{Az} - \hat{d}_{Az} \\ d_\phi - \hat{d}_\phi \end{bmatrix} - \begin{bmatrix} K_{Az} & 0 \\ 0 & K_\phi \end{bmatrix} \begin{bmatrix} \sigma_{Az} \\ \sigma_\phi \end{bmatrix} + \begin{bmatrix} \dot{v} & -\dot{u} \\ 1 & \tan\theta \sin\phi \end{bmatrix} \begin{bmatrix} \sigma_L \\ \sigma_M \end{bmatrix}$$

$$\begin{bmatrix} \dot{\sigma}_L \\ \dot{\sigma}_M \\ \dot{\sigma}_N \end{bmatrix} = \begin{bmatrix} \bar{f}_L - \hat{\bar{f}}_L \\ \bar{f}_M - \hat{\bar{f}}_M \\ \bar{f}_N - \hat{\bar{f}}_N \end{bmatrix} - \begin{bmatrix} K_L & 0 & 0 \\ 0 & K_M & 0 \\ 0 & 0 & K_N \end{bmatrix} \begin{bmatrix} \sigma_L \\ \sigma_M \\ \sigma_N \end{bmatrix}$$

$$\bar{\tau}_i \dot{\hat{\eta}}_i = -\hat{\eta}_i + \eta_i \tag{66}$$

where

$$\eta_j = d_j, \qquad \hat{\eta}_j = \hat{d}_j \quad \forall\ j = Az, \phi, \qquad \eta_k = \bar{f}_k,$$
$$\hat{\eta}_k = \hat{\bar{f}}_k \quad \forall\ k = L, M, N$$

Asymptotic convergence of the sliding variables σ_{Az}, σ_ϕ, σ_L, σ_M, and σ_N to a zone (see Theorem 2) is provided as soon as the conditions of Theorem 2 are met. The size of this zone is controlled by time constants of the filters (14) with $i = A_z, \phi, L, M$, and N and the control gains K_{Az} , K_ϕ, K_L, K_M, and K_N [full analogy to the gain matrices $\boldsymbol{K}^1$ and $\boldsymbol{K}^2$ in Eqs. (37–39)], As was stated in Secs. II and III, the same zone convergence for σ_{Az}, σ_ϕ, σ_L, σ_M, and σ_N can be established with much smaller control gain K_{Az} , K_ϕ, K_L, K_M, and K_N values rather than using a high gain control without an SMDO [10].

D. Control System Parameterization

The following choice of the system [Eq. (66)] parameters is recommended:

condition a

$$K_i > 0 \quad \forall\ i = Az, \phi, L, M, N$$

condition b

$$K_i \gg K_j \quad \forall\ j = Az, \phi$$

condition c

$$1/\bar{\tau}_i \gg K_j \quad \forall\ i = Az, \phi, L, M, N \quad \forall\ j = Az, \phi$$

The condition a is, in fact, the same as the condition b in Theorem 1, which is necessary for system stability. The condition b follows a recommendation formulated in Remark 3 that yields decoupling (time-scaling) between the inner ($\sigma_L, \sigma_M, \sigma_N$) and the outer ($\sigma_{Az}, \sigma_\phi$) loop sliding variable dynamics. Meeting this condition is useful in a practical implementation but not necessary for providing system stability (see Theorems 1 and 2). The condition c provides for the transient times in the SMDO, which basically are controlled by the time constants of the filter (14) with $i = Az$, ϕ, L, M, and N. These transients are meant to be faster than the transients in the control loops. Meeting this condition helps to reduce the effect of SMDO dynamics on the compensated dynamics of the tracking errors. All these conditions are not very restrictive and can be met in the RLV control system design.

VII. Baseline X-33 Flight Controller Design

Lockheed Martin Corporation in Houston, Texas developed the baseline X-33 guidance and control system. The guidance function varies little from the Space Shuttle reentry guidance, and the control system is similar to the Shuttle's as well. A diagram of the X-33 baseline controller is shown in Fig. 4.

The controller has three channels: roll, pitch, and yaw. In each channel, the guidance commands are smoothed and gained to form a rate command. A proportional–integral control law is then used to obtain virtual deflection commands. These are combined with aerosurface trim commands obtained from table lookup and a speed brake command generated by the guidance function, in a control mixing logic to form the individual aerosurface commands. Each channel has crossfeed paths to the other channels for the purpose of turn coordination. This feature provides a bank maneuver in response to commanded roll from guidance in such a way that ideally would force side acceleration N_y to zero. Gains are scheduled as a function of the Mach number, and commands are limited in various places in the controller. Bending filters, used to attenuate flex body effects fed back through the flight control sensors, are strategically placed. For the purpose of controller performance comparison, filter coefficients in the baseline controller were changed so that the filters simply pass the inputs through without changing magnitude or adding phase lag. This was done because flex body effects were not modeled in the simulations and no bending filters were implemented in the SMC/SMDO design.

The baseline X-33 autopilot was tested in simulation over several years to accommodate design and mission changes, higher-fidelity subsystem and environment modeling, system and environmental dispersions, and numerous failure scenarios. By the end of the X-33 program, it was at a high level of maturity and had proven it could meet vehicle and mission requirements in MAVERIC simulations with high-fidelity vehicle subsystem models. These included extensive Monte Carlo and vehicle system failures.

VIII. Flight Simulation Results and Analysis

The continuous SMC/SMDO was coded and implemented in MAVERIC and the simulation results were compared with the baseline classical controller design. Only the autopilots were different between the two simulations; all other models remained unchanged, including a second-order actuator model with position and rate limiting and the wind model.

The simulations began at the TAEM interface and terminated at the main gear touchdown on the runway. The control functions [Eq. (63)] in terms of roll, pitch, and yaw acceleration commands are transformed into virtual deflection commands by Eq. (49), allocated

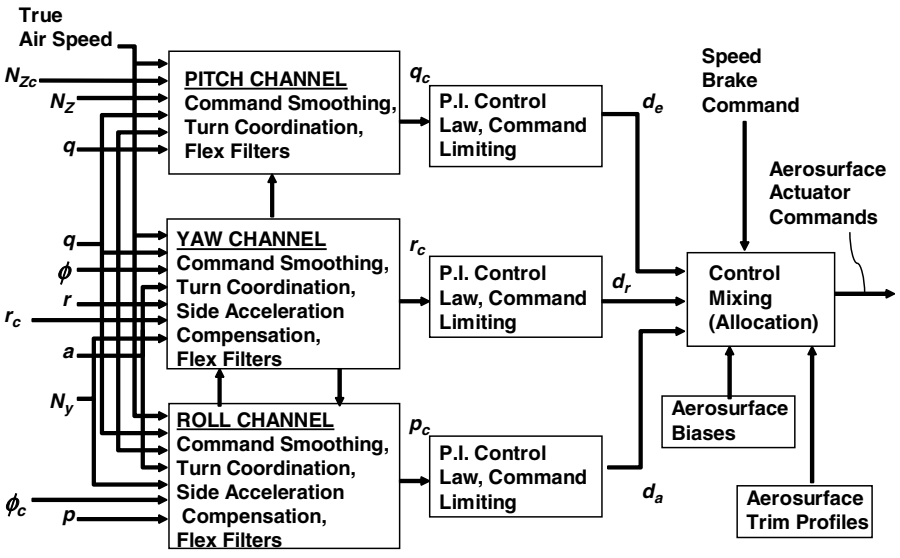

Fig. 4 Baseline X-33 controller for TAL region of flight.

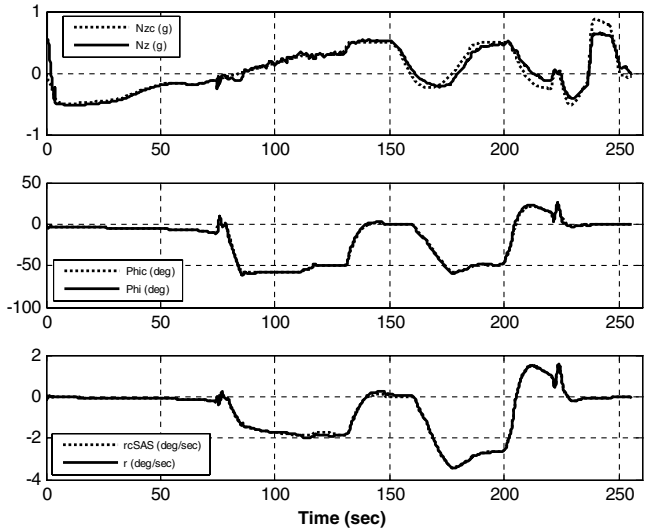

Fig. 5 Guidance command tracking via SMC with nominal wind.

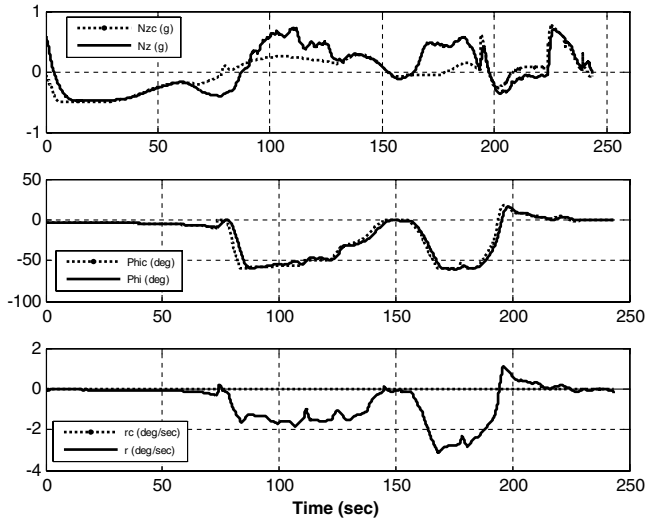

Fig. 6 Guidance command tracking via baseline controller with nominal wind.

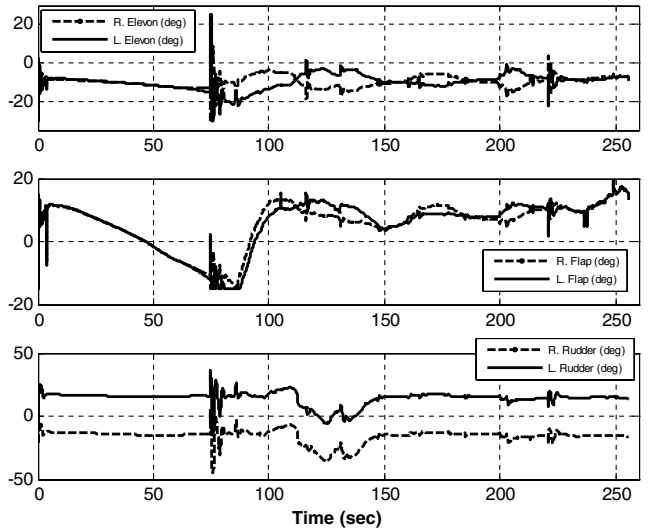

Fig. 7 Elevon, flap, and rudder deflections via SMC with nominal wind.

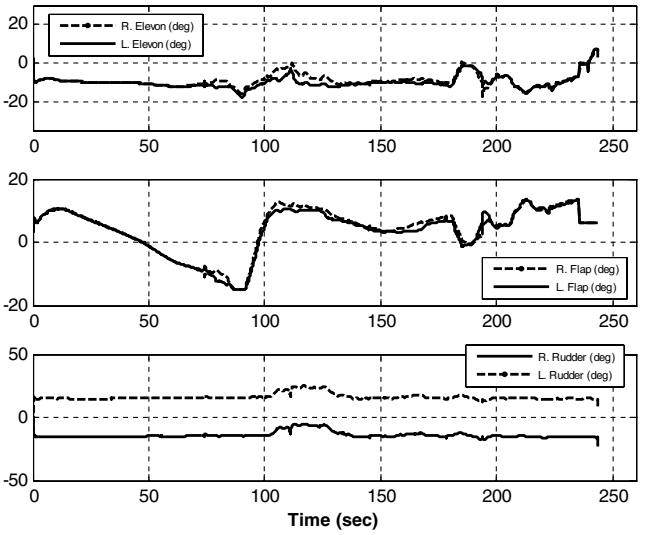

Fig. 8 Elevon, flap, and rudder deflections via baseline controller with nominal wind.

into actual actuator commands by means of the control allocator (50), and these are sent to the actuators (46).

Remark 6: Implementing virtual rate commands p_c and q_c as in Eq. (54) using the matrix $\boldsymbol{A}^1$ from Eq. (48) made tuning the normal acceleration and roll angle loops difficult due to the time-varying nature of this matrix. For the preliminary controller design, a constant identity matrix

$$\boldsymbol{A}^1 = \begin{bmatrix} 1 & 0 \\ 0 & 1 \end{bmatrix}$$

was used instead, with highly successful results.

The proposed continuous SMC/SMDO and the baseline controllers were compared in two simulation cases: one with nominal wind and one with severe headwind gust. Simulation results from the nominal wind case are shown in Figs. 5–8. In comparing Fig. 5 (SMC/SMDO) and Fig. 6 (baseline), it can be seen that normal acceleration and roll angle tracking is far better with SMC/SMDO (in particular, the roll angle command is followed almost perfectly by SMC/SMDO). The yaw rate command is also followed very well by SMC/SMDO. The baseline controller does not follow the yaw rate command, which is always equal to zero, generated by guidance very closely due to the fact that it too uses turn coordination through interchannel crossfeeds. It should be noted that guidance command profiles are slightly different between the two simulations due to the fact that closed-loop guidance shapes its commands as a function of

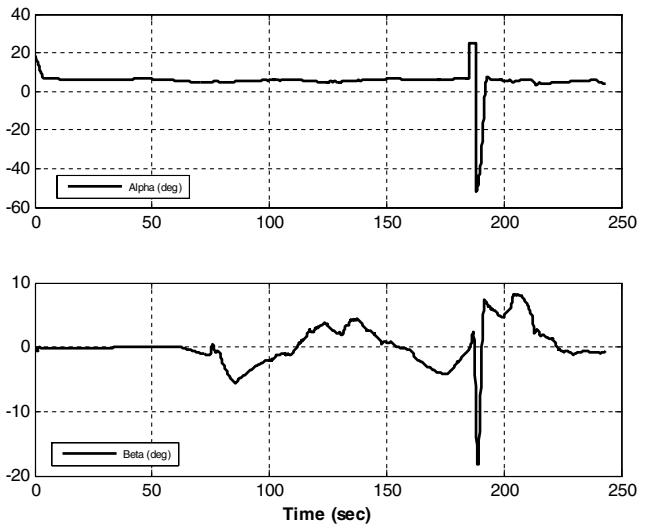

Fig. 9 Sideslip and angle of attack via SMC with severe wind gust.

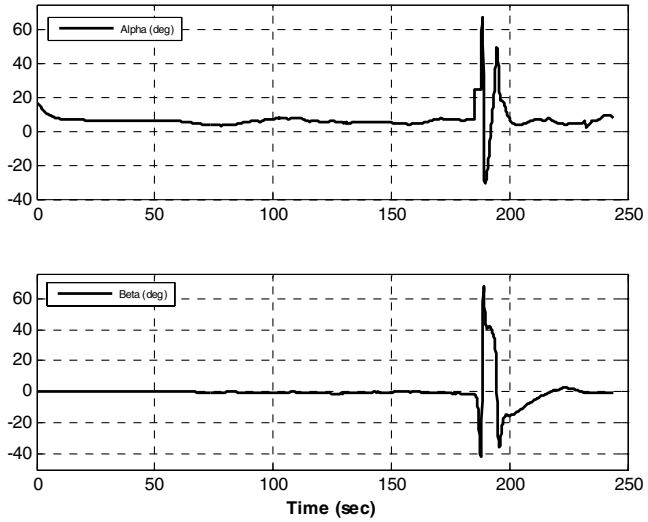

Fig. 10 Sideslip and angle of attack via baseline controller with severe wind gust.

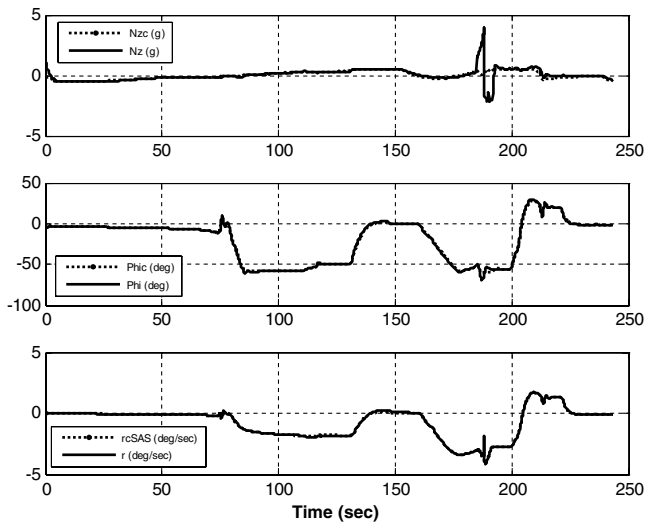

Fig. 11 Guidance command tracking via SMC with severe wind gust.

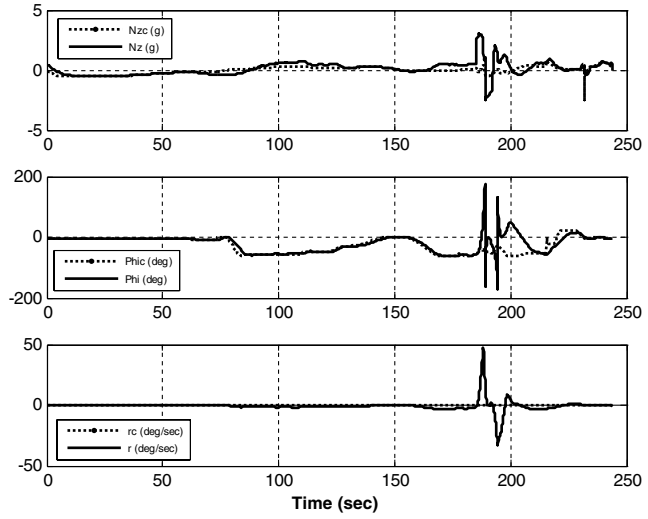

Fig. 12 Guidance command tracking via baseline controller with severe wind gust.

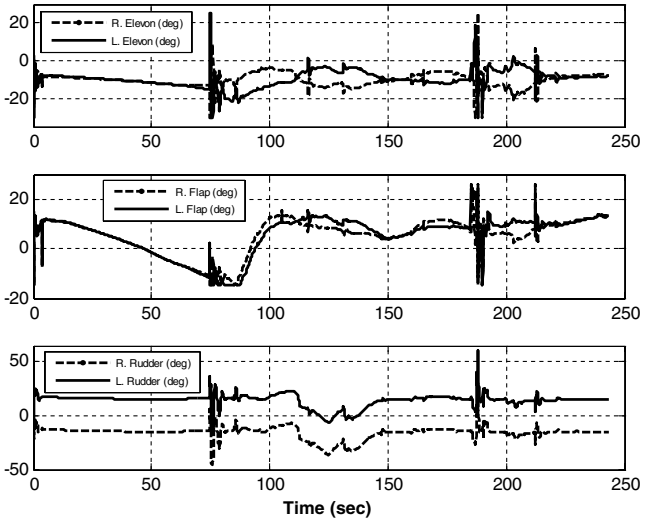

Fig. 13 Elevon, flap, and rudder deflections via SMC with severe wind gust.

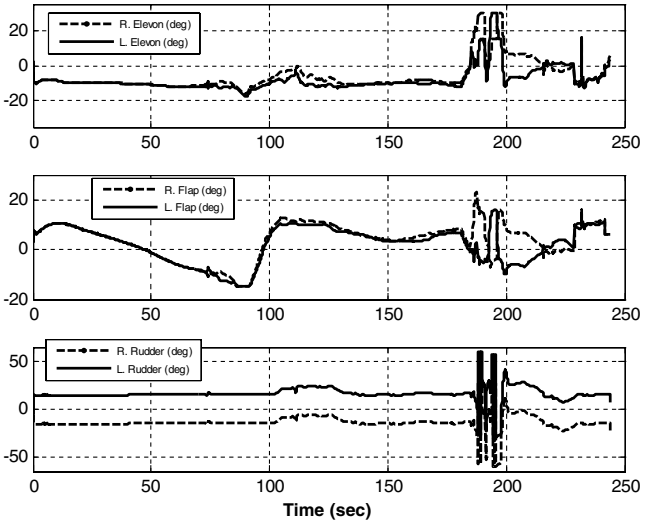

Fig. 14 Elevon, flap, and rudder deflections via baseline controller with severe wind gust.

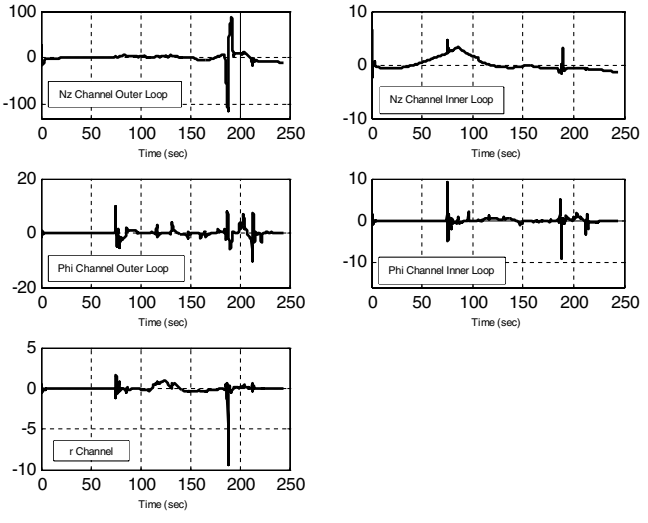

Fig. 15 SMC sliding variables with severe wind gust.

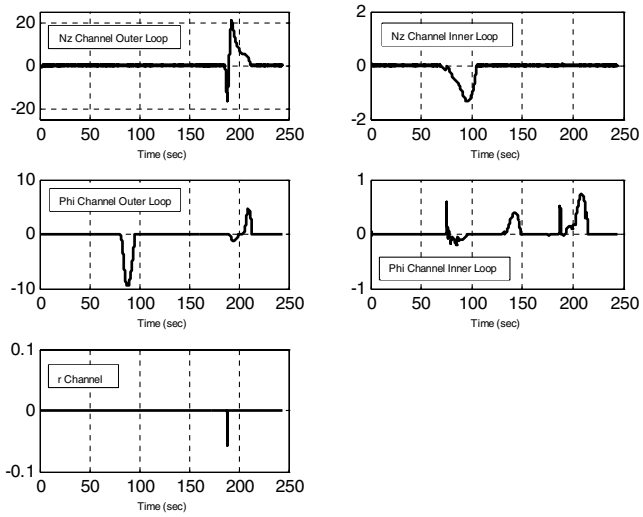

Fig. 16 SMDO sliding variables with severe wind gust.

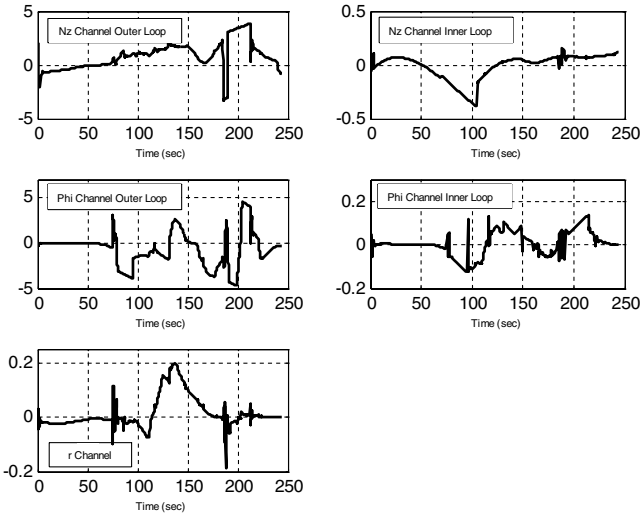

Fig. 17 SMDO disturbance estimates with severe wind gust.

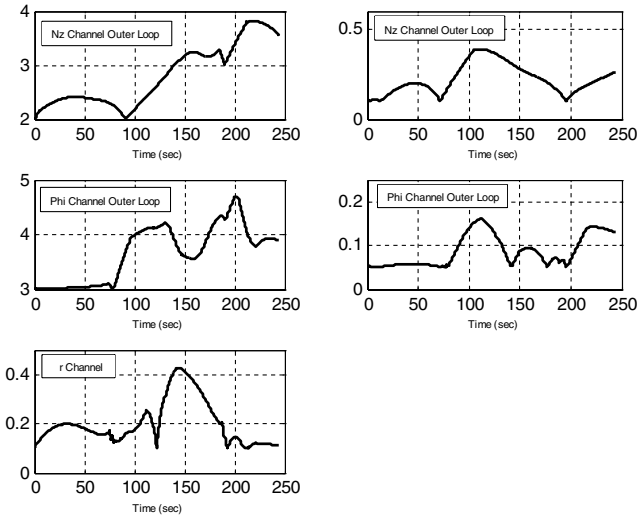

Fig. 18 SMDO adaptive gains with severe wind gust.

flight condition and distance from the landing site. Flight conditions differ because the two controllers produce different aerosurface commands, resulting in different aerodynamic accelerations on the vehicle.

The aerosurface deflections are shown in Fig. 7 for the SMC and Fig. 8 for the baseline controller. The average deflections are similar in magnitude; however, to provide more accurate guidance command tracking, the SMC commands them more aggressively due to use of SMDO in response to maneuvers and other disturbances. This results in large transient deflections that quickly decrease once the tracking error is again close to zero.

To provide a more stressing case for the control system, a severe headwind gust was simulated by artificially imposing a 25-deg angle of attack for a duration of 3 s at 185 s flight time. Simulation results for this case are shown in Figs. 9–18. The gust appears as a step increase in angle of attack in Fig. 9. The sideslip angle is also shown. The vehicle recovers from the gust and resumes a nominal alpha and beta profile by about 195 s. Alpha and beta profiles from the baseline controller simulation are shown in Fig. 10. The baseline controller departs, allowing extremely large angles of attack and sideslip to build up.

Guidance command tracking is shown in Fig. 11, SMC/SMDO, and Fig. 12, baseline controller. At the time of the wind gust, the SMC/SMDO allows roughly 4–g error in normal acceleration, while roll and yaw errors are about the same as in the nominal simulation. In the baseline controller simulation, the vehicle rolls through 360 deg and the yaw rate climbs to a maximum of 50 deg/s.

Figures 13 and 14 show aerosurface deflections for the SMC/SMDO and baseline controllers, respectively. Actuator demand is very aggressive for both simulations, although the baseline control results in actuator saturations for longer periods of time during the wind gust. Figure 15 shows sliding variables for the SMC/SMDO outer loop [Eq. (52) with $i = A_z$ and ϕ] and inner loop [Eq. (52) with $i = L$, M, and N].

Figure 16 shows sliding variables for the SMDO outer loop [Eq. (55)] and SMDO inner loop [Eq. (64)]. Sliding variables diverge occasionally due to guidance maneuvers and the wind disturbance, but then reconverge to a region around zero. The SMDO sliding variables shown are before filtering. Disturbances are mainly in pitch and roll in this simulation, so the yaw rate SMDO provides almost ideal convergence to the sliding mode ($s_N = 0$).

Outer [Eqs. (8), (14), and (57) with $i = A_z$ and ϕ] and inner [Eqs. (14), (57), and (58) with $i = L$, M, and N] loop SMDO disturbance estimates are shown in Fig. 17 and their associated adaptive gains in Eq. (58) are shown in Fig. 18. The disturbance estimates are a function of maneuver rates, wind disturbance, and other unmodeled dynamics. The adaptive gains are continuous and vary as needed to compensate for varying disturbance magnitudes and provide convergence to the sliding mode.

IX. Conclusions

A novel sliding mode control approach, continuous sliding mode control driven by sliding mode disturbance observer with gain adaptation, SMC/SMDO, is studied for cascading uncertain systems control and a reusable launch vehicle flight control system design as a way to improve robustness to many phenomena, such as modeling uncertainties and disturbances, while retaining continuity of control without using high control gains. Because of the robustness to external disturbances (including wind gusts), different mission trajectories, and modeling uncertainties, the proposed flight control system design also can reduce cost by requiring less time in design cycle and preflight analyses. This design is applied to a flight regime named terminal area energy management and approach/landing. The multiple-loop flight controller design features low-order disturbance observers that rely only on knowledge of the bounds of the disturbance. A gain-adaptation algorithm is included in the disturbance observer design that provides the least gain needed for existence of the sliding mode. The developed SMC/SMDO algorithm for the reusable launch vehicle flight control system was coded and implemented in the X-33 MAVERIC simulation. In its

implementation, problems faced in real-world applications (like filtering and multirate subsystems) were successfully addressed. The simulations began at the terminal area energy management interface and terminated at the main gear touchdown on the runway. Flight simulations of the X-33 reusable launch vehicle were performed with the Shuttle-like baseline controller and with the SMC/SMDO. Two simulation cases were studied: 1) a nominal vehicle and a reference wind model consisting of measured wind data and 2) the same vehicle models and the same wind model with a severe, artificial gust imposed. In each case, the continuous SMC/SMDO performed better in guidance command tracking. In the severe wind-gust case, the baseline controller departed in roll and yaw, whereas the SMC/SMDO did not. Although the design, implementation, and simulation results were very promising, simulations with dispersions and failures are needed to adequately compare the SMC/SMDO approach with the classical, baseline flight control system.

References

[1] Anon., "2006 NASA Strategic Plan," NASA NP-2006-02-423-HQ, Jan. 2006.

[2] Hanson, J., "New Guidance for New Launchers," *Aerospace America*, March 2003, pp. 36–41.

[3] Hanson, J., Jones, R., and Krupp, D., "Advanced Guidance and Control Methods for Reusable Launch Vehicles: Test Results," AIAA Paper 2002-4561, Aug. 2002.

[4] Hill, A., Compton, J., McCarter, J. W., "Maveric Release 2.3 User's Guide, A Software Tool for Rapid Development of High Fidelity 3-DOF/6-DOF Flight Simulation of Aerospace Vehicles," NASA, TR-FRL-111505-1, Nov. 15, 2005.

[5] Drake, D., Xin, M., and Balakrishnan, S. N., "New Nonlinear Control Technique for Ascent Phase of Reusable Launch Vehicles," *Journal of Guidance, Control, and Dynamics*, Vol. 27, No. 6, 2004, pp. 930–937.

[6] Schierman, J. D., Ward, D. G., Hull, J. R., Gandhi, N., Oppenheimer, M., and Doman, D. B., "Integrated Adaptive Guidance and Control for Re-Entry Vehicles with Flight Test Results," *Journal of Guidance, Control, and Dynamics*, Vol. 27, No. 6, 2004, pp. 975–988.

[7] Bevaqua, T., Best, E., Huizenga, A., Cooper, D., and Zhu, J., "Improved Trajectory Linearization Flight Controller for Reusable Launch Vehicles," AIAA Paper 2004-875, Jan. 2004.

[8] Shtessel, Y. B., and Hall, C. E., "Sliding Mode Control of the X-33 with an Engine Failure," AIAA Paper 2000-3883, Jul. 2000.

[9] Shtessel, Y., Tournes, C., and Krupp, D., "Reusable Launch Vehicle Control In Sliding Modes," AIAA Paper 97-3533, Aug. 1997.

[10] Shtessel, Y., Hall, C., and Jackson, M., "Reusable Launch Vehicle Control in Multiple-Time-Scale Sliding Modes," *Journal of Guidance, Control, and Dynamics*, Vol. 23, No. 6, 2000, pp. 1013–1020.

[11] Shtessel, Y. B., and Hall, C. E., "Multiple Time Scale Sliding Mode Control of Reusable Launch Vehicles in Ascent and Descent Modes," *Proceedings of the IEEE American Control Conference*, IEEE Publications, Piscataway, NJ, 2001, pp. 4357–4362.

[12] Shtessel, Y. B., Zhu, J. J., and Daniels D., "Reusable Launch Vehicle Attitude Control Using Time-Varying Sliding Modes," AIAA Paper 2002-4779, Aug. 2002.

[13] Hull, J., Gandhi, N., and Schierman, J., "In-Flight TAEM/Final Approach Trajectory Generation for Reusable Launch Vehicles," AIAA Paper 2005-7114, Aug. 2005.

[14] Kluever, C. A., "Unpowered Approach and Landing Guidance Using Trajectory Planning," *Journal of Guidance, Control, and Dynamics*, Vol. 27, No. 6, 2004, pp. 967–974.

[15] Kluever, C., and Horneman, K., "Terminal Trajectory Planning and Optimization for an Unpowered Reusable Launch Vehicle," AIAA Paper 2005-6058, Aug. 2005.

[16] Shtessel, Y., Buffington, J., and Banda, S., "Multiple Timescale Flight Control Using Reconfigurable Sliding Modes," *Journal of Guidance, Control, and Dynamics*, Vol. 22, No. 6, 1999, pp. 873–883.

[17] Shtessel, Y., Buffington, J., and Banda, S., "Tailless Aircraft Flight Control Using Multiple Time Scale Re-Configurable Sliding Modes," *IEEE Transactions on Control Systems Technology*, Vol. 10, No. 2, 2002, pp. 288–296.

[18] Shkolnikov, I., Shtessel, Y., Lianos, D., and Thies, A., "Robust Missile Autopilot Design Via High Order Sliding Mode Control," AIAA Paper 2000-3986, Aug. 2000.

[19] Shkolnikov, I., Shtessel, Y., and Lianos, D., "Integrated Guidance-Control System of a Homing Interceptor: Sliding Mode Approach," AIAA Paper 2001-4218, Aug. 2001.

[20] Utkin, V., Guldner, J., and Shi, J., *Sliding Mode Control in Electromechanical Systems*, Taylor and Francis, London, 1999, pp. 51–145.

[21] Massey, T., and Shtessel, Y., "Continuous Traditional and High Order Sliding Modes for Satellite Formation Control," *Journal of Guidance, Control, and Dynamics*, Vol. 28, No. 4, 2005, pp. 826–831.

[22] Isidori, A., *Nonlinear Control Systems*, 3rd ed., Springer–Verlag, Berlin, 1995, pp. 31–140.

[23] Poularikas, A. D., and Seely, S., *Signals and Systems*, PWS Publishing, Boston, 1985, pp. 352–361.

[24] Kuo, B. C., *Digital Control Systems*, Oxford Univ. Press, Oxford, 1992, pp. 225–229.

[25] Levant, A., "Universal Single-Input-Single-Output (SISO) Sliding-Mode Controllers with Finite-Time Convergence," *IEEE Transactions on Automatic Control*, Vol. 46, No. 9, 2001, pp. 1447–1451.

[26] Polycarpou, M., "Stable Adaptive Neural Control Scheme for Nonlinear Systems," *IEEE Transactions on Automatic Control*, Vol. 41, No. 3, 1996, pp. 447–451.

[27] Swaroop, D., J., Hedrick, K., Yip, P. P., and Gerdes, J. C., "Dynamic Surface Control for a Class of Nonlinear Systems," *IEEE Transactions on Automatic Control*, Vol. 45, No. 10, 2000, pp. 1893–1899.

[28] Shkolnikov, I. A., and Shtessel, Y. B., "A Multiple-Loop Sliding Mode Control System with Second-Order Boundary Layer Dynamics," *Proceedings of the IFAC World Congress* [CD ROM], Elsevier, Amsterdam, 2002; also International Federation of Automatic Control Paper 597.

[29] Slotine, J-J., and Li, W., *Applied Nonlinear Control*, Prentice–Hall, Upper Saddle River, NJ, 1991, pp. 276–310.

[30] Wise, K. A. and Broy, D. J., "Agile Missile Dynamics and Control," *Journal of Guidance, Control, and Dynamics*, Vol. 21, No. 3, 1998, pp. 441–449.

[31] Blakelock, J. H., *Automatic Control of Aircraft and Missiles*, 2nd ed., Wiley, New York, 1991, pp. 333–344.